



Water Resources Research

RESEARCH ARTICLE

10.1029/2020WR028401

Key Points:

- Swash motion on beaches with heterogeneous sediments leads to capillary barriers and moisture hotspots beneath the beach surface
- Strain-dominated and vorticity-dominated flow regions coexist at small spatial scales within the swash zone due to geologic heterogeneity
- Heterogeneity creates both high and low mixing spots in subsurface flow percolating from the swash zone into the porous media

Correspondence to:

M. C. Boufadel,
boufadel@gmail.com

Citation:

Geng, X., Heiss, J. W., Michael, H. A., Boufadel, M. C., & Lee, K. (2020). Groundwater flow and moisture dynamics in the swash zone: Effects of heterogeneous hydraulic conductivity and capillarity. *Water Resources Research*, 56, e2020WR028401. <https://doi.org/10.1029/2020WR028401>

Received 16 JUL 2020

Accepted 23 OCT 2020

Accepted article online 29 OCT 2020

Groundwater Flow and Moisture Dynamics in the Swash Zone: Effects of Heterogeneous Hydraulic Conductivity and Capillarity

Xiaolong Geng¹ , James W. Heiss² , Holly A. Michael^{3,4} , Michel C. Boufadel¹ , and Kenneth Lee⁵

¹Department of Civil and Environmental Engineering, New Jersey Institute of Technology, University Heights, Newark, NJ, USA, ²Department of Environmental, Earth and Atmospheric Sciences, University of Massachusetts Lowell, Lowell, MA, USA, ³Department of Earth Sciences, University of Delaware, Newark, DE, USA, ⁴Department of Civil and Environmental Engineering, University of Delaware, Newark, DE, USA, ⁵Department of Fisheries and Oceans, Dartmouth, Nova Scotia, Canada

Abstract A density-dependent, variably saturated groundwater flow and solute transport model was used to investigate the influence of swash motions on subsurface flow and moisture dynamics in beach aquifers with heterogeneous distributions of hydraulic conductivity (K) and capillarity. The numerical simulations were performed within a Monte Carlo framework using field measurements conducted in the swash zone of a sandy beach. Our results show that heterogeneous capillarity causes spatially variable capillary rise above the groundwater table. In response to swash motions, heterogeneity creates capillary barriers that result in pockets of elevated moisture content beneath the swash zone. These moisture hotspots persist within the unsaturated zone even at ebb tide when the swash motions recede seaward. Heterogeneous capillarity also results in highly tortuous preferential flow paths and alters the flow rates from the sand surface to the water table. Heterogeneous K greatly enhances the seawater infiltration into the swash zone and modulates its spatial distribution along the beach surface. Due to heterogeneous K and capillarity, complex mixing patterns emerge. Both strain-dominated and vorticity-dominated flow regions develop and dissipate as tides and waves move across the beach surface. Complex mixing patterns of seawater percolating from the swash zone surface to the water table, with localized areas of high and low mixing intensities, are further demonstrated by analysis of dilution index. Our findings reveal the influence of geologic heterogeneity on swash zone moisture and flow dynamics, which may have important implications for sediment transport and chemical processing in beach aquifers.

Plain Language Summary In marine coastal environments, swash zone mixing and exchange dynamics have been identified as critical factors affecting biogeochemical cycles and nutrient loads from aquifers to coastal waters. Our results for the first time demonstrate a dynamic response of moisture and subsurface flow to swash motions in the presence of aquifer heterogeneity. Heterogeneity coupled with high-frequency wave forcing results in moisture hotspots and significant tempo-spatial variability of strain-dominated and vorticity-dominated flow regions within the swash unsaturated zone, which have important implications for biogeochemical processes and local-scale mixing rates. These results highlight the importance of considering geologic heterogeneity in both hydraulic conductivity and capillarity in studies of groundwater flow and solute transport processes in coastal beach aquifers subjected to swash motions.

1. Introduction

The swash zone is an important region on the beach that controls intertidal benthic community structure and biodiversity (Gray et al., 2014; McArdle & McLachlan, 1992). Previous studies have revealed that complex groundwater mixing occurs in the swash zone due to high-frequency inundation and seawater infiltration by individual waves (Cartwright et al., 2002; Geng et al., 2014, 2017; Geng & Boufadel, 2015; Heiss et al., 2014; Malott et al., 2017; Xin et al., 2010). Swash and tidal action are a primary control on near-shore biogeochemical processes and submarine discharge of various chemical species (e.g., nutrients, carbon, arsenic, and trace elements) into coastal waters (Boehm et al., 2006; Brown & Boehm, 2016; Kim

et al., 2017; Lässig, 2019; Mohapatra et al., 2011; Praveena et al., 2012; Rakimbekova et al., 2018; Waska, 2019). Kim et al. (2020) revealed that intertidal groundwater-seawater mixing driven by tides likely creates a dynamic reactive circulation cell, where areas with high denitrification rates shift landward and seaward along the mixing zone through spring-neap cycles. Total denitrification in beach aquifers can yield nitrate removal efficiencies of >90% for typical ocean forcing and beach characteristics (Anwar et al., 2014; Heiss et al., 2017). The elevated reaction rates are supported by tide- and swash-driven infiltration that supplies organic matter and mineralization products to the beach subsurface through the unsaturated zone (Anschatz et al., 2009; Ullman et al., 2003). Thus, it is important to characterize unsaturated flow in beach sediments to more accurately estimate the role of beach aquifers on moderating chemical fluxes to the coastal zone.

The rapid change of moisture content due to swash motions has strong implications on the spatial distribution and population dynamics of fauna inhabiting the interstitial sand matrix (de Alava & Defeo, 1991; Defeo & McLachlan, 2005; McLachlan, 1983). For example, in marine sediments, moisture content has been identified as a critical factor affecting biogeochemical processes (e.g., N mineralization) (Jia et al., 2019; Tian et al., 2010; Yin et al., 2019), and modulating the composition, motility, and survival of microorganisms responsible for biodegradation of contaminants (Yadav & Hassanzadeh, 2011). Studies revealed that the rate of N mineralization varies greatly with soil moisture content, and the optimal moisture content for the mineralization appears to be 80%–100% of field capacity (Cassman & Munns, 1980; Guntiñas et al., 2012). Other studies have demonstrated that air flow through the unsaturated zone to the water table can drive nitrification at the water table in beach sediments (Schutte et al., 2018). Because moisture content in the unsaturated zone affects the connection between the water table and atmosphere, pore water oxygen supply and nitrification in beaches is also likely controlled by saturation dynamics from wave swash. It is therefore important to accurately characterize spatial and temporal patterns of moisture content in shallow intertidal sediments to quantify N mineralization and cycling within beach aquifers. Current understanding of moisture content in intertidal sediments assumes homogeneous capillarity and hydraulic conductivity; however, heterogeneity of these aquifer characteristics is likely to create moisture content hotspots, potentially elevating N mineralization rates while reducing nitrification due to restricted air flow in the unsaturated zone. The extent of these moisture content controls on biogeochemical processes in beaches remains unclear and is not accounted for in current conceptual and mathematical models of beach groundwater systems.

Over the past four decades, considerable efforts have been made to investigate groundwater dynamics in response to swash motions (Horn, 2002, 2006; Robinson et al., 2018; Santos et al., 2012). Longuet-Higgins and Smith (1983) performed laboratory experiments to illustrate wave effects on groundwater flow in the surf and swash zones. Their experimental results demonstrated that a groundwater circulation pattern forms beneath the beach that extends from the lower end of the swash zone to the surf zone. Boufadel et al. (2007) conducted tracer studies in a laboratory beach facility to investigate the influence of waves on subsurface pollutant mixing and transport processes. Their results showed that waves create a steep hydraulic gradient in the swash zone, which increases the residence time of the tracer plume and greatly alters the transport of solutes prior to discharge. Sous et al. (2013) carried out experiments in a wave basin and found that pressure gradients observed under the swash zone are mainly driven by wave-induced infiltration. Turner et al. (2016) performed a large-scale laboratory experiment to investigate groundwater fluxes and flow paths in beaches subjected to waves. Results showed that groundwater levels, flow paths, and fluxes within the beach face are predominantly controlled by the action of waves, regardless of the overall seaward- or landward-directed barrier-scale hydraulic gradient. Besides laboratory setups, few field studies have been conducted to investigate swash zone groundwater dynamics. Atherton et al. (2001) monitored water content within the uppermost portions of beach sediments located on the southwest coast of Anglesey, northwest Wales, UK, where substantial horizontal movement of pore water through the capillary fringe has been identified. Heiss et al. (2014, 2015) conducted field studies to investigate swash zone moisture dynamics and unsaturated infiltration in two sandy beaches at Cape Henlopen, DE, USA. The studies revealed a dynamic response of moisture content in the unsaturated region of the swash zone to wave overtopping and swash infiltration. Sous et al. (2016) carried out a field experiment on a microtidal beach and revealed the presence of a rather consistent groundwater circulation pattern under the swash zone. Heiss, Michael, and Puleo (2020) demonstrated that the lens of infiltrating seawater that moves downward through the unsaturated

zone to the water table, contributing to the formation of the circulation cell, moves landward and seaward as the tide and swash zone move across the beach surface.

Numerical studies have also been widely conducted to characterize swash zone dynamics. Modeling groundwater and solute transport dynamics coupled with wave forcing is computationally expensive due to the need to explicitly model the sea surface and velocity field at extremely high temporal and spatial resolutions. Phase-resolving modeling of surface waves including explicit reproduction of the sea surface and velocity field evolution is often achieved by coupling turbulence models (e.g., $k-\epsilon$ model, $k-\omega$ model, and Reynold stress equation model) and volume of fluid (VOF) techniques (Hirt & Nichols, 1981; Wilcox, 1993, 1998). The former is used to simulate flow characteristics under turbulent condition, and the latter is used to predict multiphase free-surface flow. Bakhtyar et al. (2011) simulated waves using the VOF technique and a $k-\epsilon$ turbulence model and then coupled the wave model to the saturated groundwater flow model SEAWAT-2000 to investigate wave-induced groundwater flow, sediment transport, and beach profile change. Geng et al. (2014) performed phase-resolving modeling of wave motions in a computational fluid dynamics (CFD) framework and then coupled the simulated wave results to a variably saturated density dependent groundwater model MARUN (Boufadel et al., 1999), to simulate swash zone groundwater flow and terrestrial solute transport processes. The study was based on tracer experiments conducted in a laboratory beach system in Boufadel et al. (2007) and further quantified the impacts of hydraulic conductivity (K) and capillarity on the migration of the tracer plume beneath the swash zone. Geng et al. (2017) performed site-specific numerical simulations to explore subsurface flow and moisture dynamics in response to swash motions; in the study, wave-induced high-frequency pressure oscillations measured in the swash zone in Heiss et al. (2015) were interpolated and used for groundwater simulations. The computational challenge of using phase-resolving wave simulations to study groundwater processes can be overcome by upscaling groundwater flow and solute transport in beach aquifers subjected to waves. For example, Xin et al. (2010) developed a phase-averaged approach where wave effects were represented by a wave-induced onshore hydraulic gradient above the mean sea level, referred to as wave setup. This approach has been used in numerous wave relevant studies (Anwar et al., 2014; Malott et al., 2017; Rakhimbekova et al., 2018; Robinson et al., 2014). Geng and Boufadel (2015) developed a “net inflow” approach to upscale wave effects on subsurface flow and transport processes. In that approach, spatially varying infiltration rates along the beach surface averaged over several wave periods were adopted as inflow boundary conditions to represent wave forcing. While the aforementioned upscaling approaches greatly reduce computational costs, the response of subsurface flow and moisture content to individual waves cannot be captured, and therefore, the phase-resolving approach is still essential for exploring swash zone dynamics.

Groundwater flow and solute transport processes can exhibit significant tempo-spatial variations in heterogeneous porous media (Adams & Gelhar, 1992; Dagan, 2012; Dentz et al., 2011; Gelhar, 1993). Pronounced spatial variability in permeability could lead to chaotic pore-water flow patterns that are similar to turbulent fields where velocity variations produce radically different flow paths of fluid particles that are initially adjacent to each other (Weeks & Sposito, 1998). de Barros et al. (2012) introduced the Okubo-Weiss parameter Θ to characterize local mixing strength in subsurface flow fields. The parameter Θ is defined in Okubo (1970) and Weiss (1991), reflecting the relative strength of fluid rotation to strain. In strain-dominated flow regions, fluid flow experiences stretching and deformation (i.e., change in fluid shape) by normal and shear strain that intensifies local mixing strength, while in vorticity-dominated flow regions, the fluid flow experiences local rotation that can be measured by the curl of the velocity vector, resulting in relatively low mixing strength. Dentz et al. (2018) further showed that the solute plume experiences spatially varied stretching-shearing deformation as it moves through a heterogeneous porous medium that complexes solute mixing with ambient fluid. Geng et al. (2020b) identified the vortex structures in 3-D groundwater flow through heterogeneous permeability fields and found that these vortex flow structures exhibit scale-invariant features in both fractal permeability fields and stationary permeability fields below the correlation scale.

The effects of heterogeneity on flow and transport behavior become more complicated in the unsaturated zone. For example, a capillary barrier that restricts flow will form when fine-grained sediment overlays coarser-grained sediment (Nicholson et al., 1989; Ross, 1990). Such a configuration generates sufficient capillary tension to limit the downward movement of water from the finer sediment layer to the coarser sediment layer, which has implications for various sorption processes (Bradford et al., 1998; Rooney et al., 1998; Stormont & Anderson, 1999). Rooney et al. (1998) performed microcosm studies to assess the role of

capillary barriers on isolating salt contaminated soils. Results showed that a 15-cm-thick layer of sandy-clay soil overtop a salt contaminated soil could effectively prevent water and salt from migrating upward into the topsoil. von Jeetze et al. (2020) investigated the role of spatial heterogeneity of K and capillarity in affecting root water uptake from unsaturated soil. Numerical simulations of water flow toward the root layer were conducted with randomized heterogeneous fields; a simple linear correlation was assumed between height of the capillary fringe and saturated K . Their results revealed that an increase in heterogeneity at the root-soil interface leads to high root water uptake rates. While a number of previous studies have explored the effects of geologic heterogeneity on flow and transport processes in coastal aquifer systems, the studies only considered spatial variability in K (Geng et al., 2020b; Geng & Michael, 2020; Heiss, Michael, & Koneshloo, 2020; Lu et al., 2013; Michael et al., 2016; Pool et al., 2015; Sebben et al., 2015). In coastal aquifers, due to oceanic forcing (e.g., tides and waves), variably saturated conditions are ubiquitously observed in nearshore beach systems; therefore, it is important to consider heterogeneity of sediment capillarity when investigating coastal flow and transport processes. Furthermore, to our knowledge, pore-water flow and moisture content dynamics at the swash time scale in beach sediments with heterogeneous K and capillarity have also not been studied.

The objective of this paper is to evaluate the effects of heterogeneous hydraulic conductivity and capillarity on swash zone groundwater flow and moisture dynamics. Specifically, the numerical study presented herein is based on a field study conducted on a beach with wave swash (Heiss et al., 2015). Simulations of subsurface flow and salt transport were conducted through a 2-D density-dependent variably saturated model within a Monte Carlo framework. Two types of heterogeneous K fields were considered without and with heterogeneous capillarity. For comparison, an additional simulation was performed with a homogeneous K field with the same geometric mean as the heterogeneous sediments. Tempo-spatial patterns of swash zone pore-water flow and moisture content in response to individual waves were quantified to understand the controls of geologic heterogeneity on flow and mixing dynamics in the swash zone of beach aquifers.

2. Methods

2.1. Field Study Conducted in Heiss et al. (2015)

Field measurements were collected at a sandy (0.39-mm median grain size) beach located at Herring Point, Cape Henlopen, DE, USA. A transect of six instrument arrays of buried moisture sensors (Meter Environmental EC-5 Soil Moisture Sensors) was installed in the swash zone from 3.5 to 6.0 m landward of the high tide line. The moisture sensors were installed at 4- to 6-cm depth intervals from 2 cm below the sand surface to a maximum depth of 24 cm into the unsaturated zone. The moisture sensors logged synchronously at 5 Hz for 8 hr, starting during a rising tide when the swash zone was still landward of the transect and ending during the following ebb after the sediment experienced a full unsaturated-saturated-unsaturated cycle. Wave-induced high-frequency surface water oscillations across the transect were monitored using pressure transducers (Druck PTX 1835) mounted to each instrument array. These surface water measurements were used to determine when the transect was inundated by swash. Groundwater table fluctuations below the moisture sensors were measured to capture saturated pore pressure response to tide and swash forcing across the beach surface. Tides were semidiurnal with a mean tidal range of 1.4 m. The offshore significant wave height and period observed during the experiment was 0.89 m and 8.6 s. In this paper, we introduced heterogeneous K and capillarity to the beach system to explore effects of geologic heterogeneity on swash zone flow and moisture dynamics.

2.2. Generation of Heterogeneous K Fields

Geophysical fields have been widely observed to be self-similar or so-called scaling invariant, which is why scientists place an object with known scale (such as a ruler) in photos of geologic cross sections or in photos of land surface elevation (Bak & Creutz, 1993; Molz & Boman, 1993; Peitgen & Saupe, 1988). In this paper, heterogeneous K fields were assumed to have multifractal scaling, which captures both Gaussian and non-Gaussian statistics (Pecknold et al., 1993; Schertzer & Lovejoy, 1987). The universal multifractal (UM) model was used to generate the multifractal K fields, which has been widely used to simulate geophysical fields such as intrinsic permeability (Boufadel et al., 2000; Meng et al., 2006) and topography (Tchiguirinskaia et al., 2000). A K field at the support scale h is termed scaling if its moments of order “ s ” are a power law of h :

$$\langle K_h^s \rangle \sim h^{-W(s)} \quad (1)$$

where the function $W(s)$ is the moment scaling function. The field K is multifractal when $W(s)$ is expressed as a nonlinear concave function of “ s ,” which has been used to characterize the spatial patterns of the turbulence energy dissipation rate (Parisi & Frisch, 1985). In the UM model, the moment scaling function of a conservative K field is given by

$$W(s) = \frac{c1}{\alpha' - 1} (s^\alpha - s) \quad (2)$$

where α' is the multifractality parameter ($0 \leq \alpha' \leq 2$), representing the sparseness of the field along with the underlying statistics of $\ln K$ fields. For $\alpha' = 2$, the $\ln K$ field is Gaussian distributed, and for $\alpha' < 2$, the $\ln K$ field is no longer Gaussian, known as Levy distributed (Papoulis, 1991). The parameter $c1$ is the codimension of the mean field, representing the intermittency (i.e., sudden large changes in K) of the field along with the spread of the underlying statistical distribution of $\ln K$. For $\alpha' = 2$, $c1$ is equal to half of the variance of $\ln K$, while for $\alpha' < 2$, theoretical moments of order α' do not exist.

In this paper, a parameter set of ($\alpha' = 2.0$, $c1 = 0.1$) was selected for generating the K field, indicating a log-normally distributed heterogeneous field with a moderate variance. Note that the assumption of log-normal permeability field (i.e., $\alpha' = 2.0$) has been widely used in groundwater flow studies (de Barros et al., 2012; Nötinger, 2000; Siena & Riva, 2018), and the spatial variance of 0.05 (i.e., $c1 = 0.1$) falls into the literature values reported for a wide range of heterogeneous aquifers, varying from 0.005 to 0.23 (Boufadel et al., 2000; Tennekoorn et al., 2003). The heterogeneous K fields were generated with 512×512 cells at $5 \text{ cm} \times 5 \text{ cm}$ resolution, and the central 140×50 cells were extracted according to the size of the simulation domain used for groundwater and solute transport simulations. Thirty K realizations were generated, with the same geometric mean of $2.4 \times 10^{-4} \text{ m/s}$. In variably saturated porous media, actual hydraulic conductivity is equal to $k_r K$, where k_r denotes relative permeability. The relative permeability k_r is related to the soil moisture ratio by the Van Genuchten (1980) model as follows:

$$k_r = S_e^{1/2} \left[1 - \left(1 - S_e^{1/m} \right)^m \right]^2 \quad (3)$$

where $m = 1 - 1/n$, and n represents the uniformity of the pores; S_e denotes the effective saturation rate, given by

$$S_e = \frac{S - S_r}{1 - S_r} = \left[\frac{1}{1 + \alpha |\psi|^n} \right]^m \quad (4)$$

where S_r is the residual saturation ratio; α is the inverse of the air-entry value, representing an estimate of the thickness of the capillary fringe. Following von Jeetze et al. (2020), parameter α was used to reflect spatial heterogeneity of capillarity properties, and a linear correlation was assumed between α and K

$$\frac{K}{K_0} = (1 + 0.1R_N) \frac{\alpha}{\alpha_0} \quad (5)$$

where K_0 and α_0 denote the geometric mean of the fields and R_N is uniformly distributed random variable between 0 and 1, accounting for certain perturbation of the correlation. In this paper, two types of heterogeneous K fields are considered: without and with heterogeneity in capillarity, labeled as heterogeneous K and heterogeneous K and α , respectively. The same homogeneous system simulated in Geng et al. (2017) is also presented herein for comparison.

2.3. Groundwater Flow and Solute Transport Model

Groundwater flow and salt transport in the swash zone were simulated using the variably saturated density dependent model MARUN (Boufadel et al., 1999), taking into account geological heterogeneity for both hydraulic conductivity and capillarity, which is, to authors' knowledge, the first study of incorporating heterogeneity effects into variably saturated flow subjected to waves. The simulated domain represented a 2-D cross section of a beach aquifer, which was 2.5 m long and ~6 m deep, extending horizontally from the landward to seaward instrument arrays (Figure 1a). The mesh resolution was ~5 cm in the horizontal direction

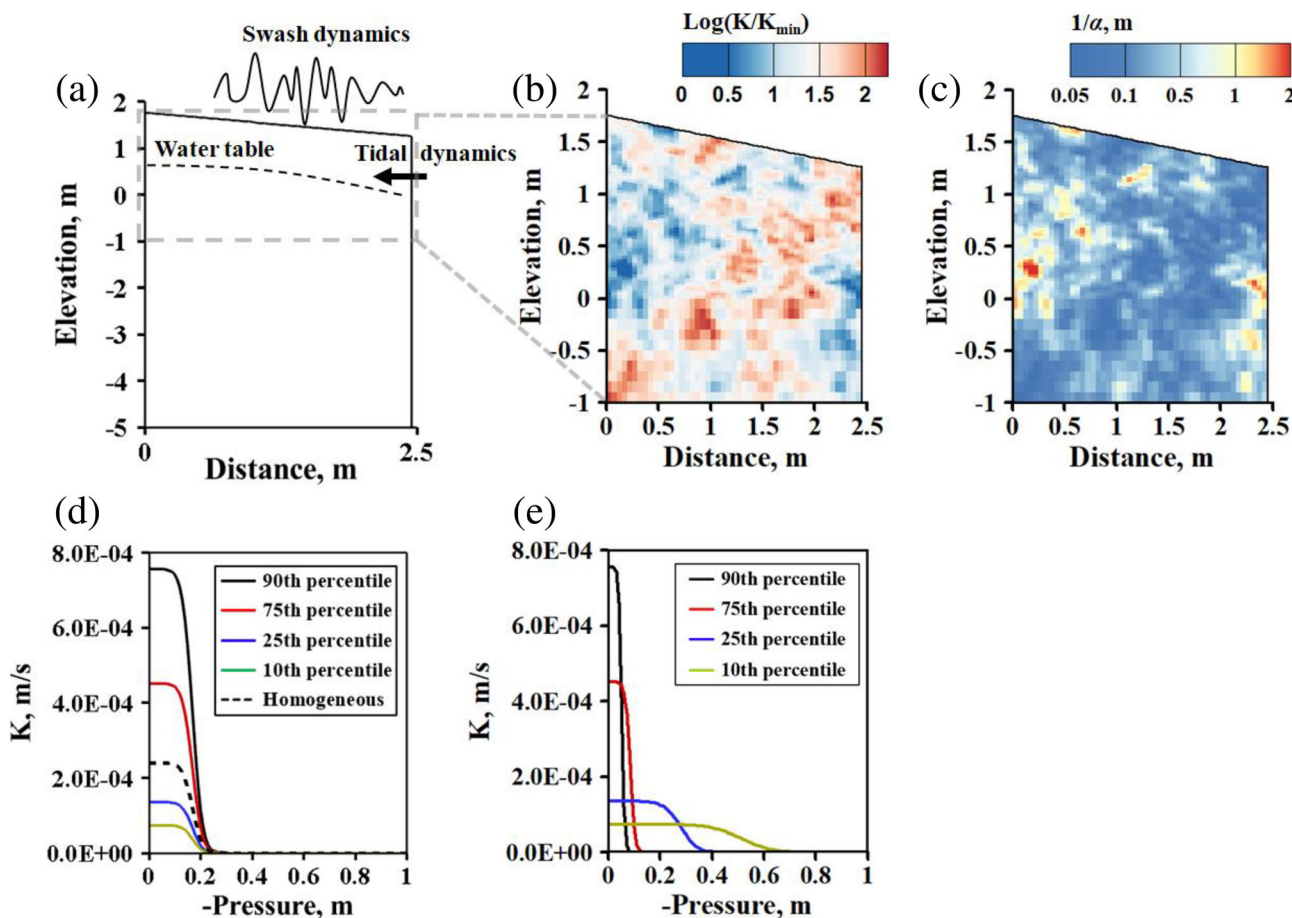


Figure 1. (a) Schematic of simulated model domain; (b and c) example saturated hydraulic conductivity (K) and $1/\alpha$ (i.e., height of capillary fringe as the porous media is unsaturated) fields; (d and e) example K as a function of pressure potential for simulated cases of heterogeneous K and K and α , without (d) and with (e) capillary heterogeneity effects. A pressure of zero indicates saturated conditions, while negative pressure indicates unsaturated conditions.

and vertically ~ 2 and ~ 5 cm above and below elevation $z = 0$, respectively. Observed water table fluctuations from the most landward and seaward pressure transducers were used as landward and seaward boundary conditions, respectively. The pressure data measured by the transducers at the sand surface were interpolated across the transect and assigned at each surface node to represent swash forcing during the 8-hr (real-time) simulation period. A constant salinity of 5.0 g/L was assigned at the landward boundary. Note that the salinity implemented at the inland boundary is slightly higher than freshwater salinity (0 g/L). However, as swash motions, rather than density differences, mainly drive seawater infiltration into the beach from the sand surface, such salinity discrepancy is unlikely to play a role in altering swash zone groundwater and moisture dynamics. The model performed a check on the beach face boundary: a Dirichlet boundary condition of 35.0 g/L was assigned for inflowing seawater, and a Neumann boundary with zero gradient was assigned when water exited the model domain. For all simulations, the model was first run for ~ 10 days with tides only until hydraulic heads and salinity reached a quasi-steady state. The resulting pore pressure and salinity distributions were used as initial conditions for the simulations with swash motions. The time step was automatically adjusted by the model to ensure convergence criteria was met (Courant number < 1). This numerical scheme has been studied and validated in earlier studies of groundwater dynamics in homogeneous sediments in the swash zone (Geng et al., 2017). The parameter values used for the simulations are reported in Table 1.

2.4. Metrics of Groundwater Flow

In heterogeneous porous media, spreading and dilution of a solute are quite different due to enhanced tortuosity of solute transport paths. The spreading of a solute plume involves stretching and

Table 1
Model Parameter Values Used in the Numerical Simulations

Symbol	Definition	Units	Value
α_0	Sand capillary fringe parameter of the Van Genuchten (1980) model	m^{-1}	5.0
n	Sand grain size distribution parameter of the Van Genuchten (1980) model	—	7.9
K_0	Saturated freshwater hydraulic conductivity	ms^{-1}	2.4×10^{-4}
α_L	Longitudinal dispersivity	m	0.04
α_T	Transverse dispersivity	m	0.004
ξ	Fitting parameter of density concentration relationship	lg^{-1}	7.44×10^{-4}
S_0	Specific storage	m^{-1}	10^{-5}
S_r	Residual soil saturation	—	0.1
Φ	Porosity ^a	—	0.37
CONVP	The convergence criterion of pressure head in the Picard iterative scheme of MARUN code	m	10^{-5}
τD_m	Product of tortuosity and diffusion coefficient	m^2s^{-1}	10^{-9}

^aNote that an average porosity of 0.37 was adopted for all the simulations.

deformation, while dilution is associated with an increase in the volume of the fluid occupied by a specified mass of solute (Kitanidis, 1994). A local-scale analysis of mixing relies on the measure of dilution, defined as the dilution index (Kitanidis, 1994), which has been recognized as a critical parameter describing solute transport through heterogeneous porous media (de Barros et al., 2012; Dentz et al., 2018). The dilution index can be linked to flow topology defined using the Okubo-Weiss parameter (Okubo, 1970; Weiss, 1991), expressed as follows:

$$\Theta = s_n^2 + s_s^2 - \omega^2 \quad (6)$$

where s_n and s_s are the normal and shear components of strain and ω is the relative vorticity of the flow, defined respectively by

$$s_n = \frac{\partial q_x}{\partial x} - \frac{\partial q_z}{\partial z} \quad (7)$$

$$s_s = \frac{\partial q_z}{\partial x} + \frac{\partial q_x}{\partial z} \quad (8)$$

$$\omega = \frac{\partial q_z}{\partial x} - \frac{\partial q_x}{\partial z} \quad (9)$$

where q_x and q_z denote the pore-water velocity in the x and z direction, respectively. The value of Θ allows separation of the flow fields into three types: a vorticity-dominated region ($\Theta < -0.2\sigma_{ow}$), a strain-dominated region ($\Theta > 0.2\sigma_{ow}$), and a background sheared flow field ($|\Theta| \leq 0.2\sigma_{ow}$), characterized by the value of σ_{ow} which is the standard deviation of the Θ field (Isern-Fontanet et al., 2004). The dilution index, $E(t)$, can then be expressed as follows (de Barros et al., 2012; Kitanidis, 1994):

$$\text{For } \Theta > 0, E(t) = \frac{4\pi|D|^{1/2}e}{\Theta^{1/2}} \sqrt{\frac{2(s_n^2 + s_s^2)}{\Theta}} [\cosh(\sqrt{\Theta}t) - 1] - (\omega t)^2 \quad (10)$$

$$\text{For } \Theta < 0, E(t) = \frac{4\pi|D|^{1/2}e}{|\Theta|^{1/2}} \sqrt{\frac{2(s_n^2 + s_s^2)}{|\Theta|}} [\cos(\sqrt{|\Theta|}t) - 1] + (\omega t)^2 \quad (11)$$

where $|D|$ is the determinant of the dispersion tensor and e is natural base. In general, where the flow region is strain dominated, the dilution index increases exponentially with time, indicating a strong increase in local mixing, and where the flow region is vorticity dominated, the dilution index is linear with time (de Barros et al., 2012; Dentz et al., 2018). Thus, a subsurface solute plume often experiences a higher mixing (i.e., dilution) in the strain-dominated region and tends to experience less mixing when it migrates through the vorticity-dominated region. In this paper, to further quantify local-scale mixing in swash zone, spatial-dependent E is calculated as follows:

$$E(x, z) = \int_0^t \frac{dE(x, z, t)}{dt} dt \quad (12)$$

where the integration is calculated at each cell for a particular length of time (e.g., 60 s, approximately 6–7 swash cycles) to represent the local-scale dilution rate at that location during that particular time period.

The probability of E higher than a threshold E_0 occurring within the swash zone for a specific time, $P_{E_0}(x, z)$, was calculated to quantify the spatial variability of the dilution index, which is defined as follows:

$$P_{E_0}(x, z) = \frac{\sum_{i=1}^N p_i(x, z)}{N} \times 100\% \quad (13)$$

where $p_i(x, z)$ is an indicator of relatively high dilution at location (x, z) of the i th geologic realization, which is equal to 1 when E is larger than E_0 , and equal to 0 for the rest; N denotes the total number of geologic realizations.

3. Results

Heterogeneity in capillarity greatly increases the spatial variability of moisture content and therefore hydraulic conductivity. Note that the hydraulic conductivity is calculated based on $k_r K$, where the relative permeability k_r varies between 0 and 1, representing variably saturated conditions, and is equal to 1 when porous media are fully saturated, and K represents saturated hydraulic conductivity (Equation 3). As shown in Figures 1b and 1c, for each simulated model cell, a higher K leads to a lower theoretical capillary fringe (i.e., $1/\alpha$) height due to the linear relation between K and the van Genuchten parameter α in Equation 5. Heterogeneous K and capillarity (labeled as heterogeneous K and α) has a stronger impact on actual hydraulic conductivity compared to the homogeneous α and K system (labeled as homogeneous case) and homogeneous α and heterogeneous K system (labeled as heterogeneous K). Figures 1d and 1e show the actual value of hydraulic conductivity as a function of pore pressure for heterogeneous K and heterogeneous K and α , respectively, calculated based on Equations 3 and 4. The selection of percentile K values from the heterogeneous fields is to demonstrate effects of heterogeneous K and α on actual hydraulic conductivity over a broad range. Note that a constant α value of 5.0 was adopted for heterogeneous K , while heterogeneous α (i.e., as a function of saturated hydraulic conductivity K , refer to Equation 5) was adopted for heterogeneous K and α . With homogeneous capillarity, either for heterogeneous K or for the homogeneous case, for different K percentiles in heterogeneous fields, hydraulic conductivity exhibits a similar response to change of pressure potential under variably saturated conditions (Figure 1d). For both the heterogeneous K and homogeneous cases, the hydraulic conductivity remains at its saturated value for each K percentile as long as the pressure potential is above -0.15 m and then sharply decreases to zero as the pressure potential drops from -0.15 to -0.3 m. In contrast, for heterogeneous K and α , hydraulic conductivities exhibit a different response to changes in pressure potential (Figure 1e). For example, there is a sharp drop in hydraulic conductivity for high percentiles of K (i.e., high K values) when the pressure drops from 0 to -0.15 m, while for low K percentiles (i.e., low K values), hydraulic conductivity decreases gradually over a wider pressure range. In effect, the sediment at 10th percentile K can maintain full saturation at lower pressures (as low as -0.4 m) relative to higher K sediment (e.g., 75th percentile K), which begins to drain at a pressure of -0.1 m.

Heterogeneity of capillarity greatly affects the tempo-spatial evolution of swash zone moisture content over a tidal cycle relative to homogeneous sediment (Figure 2). In the homogenous model case, moisture content in the upper 25 cm of the beach increases when swash events are large enough to inundate the sand surface within the model domain and result in seawater infiltration (time $t = 1.5$ h). The area of elevated moisture content gradually expands landward and downward as the tide level moves landward, leading to more frequent swash inundation and seawater infiltration until the lens of infiltrating seawater merges with the capillary fringe at depth (Row 1; $t = 2.0, 4.5$, and 5.5 h). During ebb tide, the swash zone recedes and moisture content within the initially unsaturated region drops (Row 1; $t = 6.5$ and 7.5 h). Compared to the homogeneous case, both heterogeneous K and K and α demonstrate similar tempo-spatial patterns of moisture content in response to swash motions. However, marked perturbation of the moisture content in all regions of the unsaturated zone is observed by detecting moisture hotspots almost at all stages of the swash motions, particularly for heterogeneous K and α (Figure 2). Due to heterogeneous capillarity, the thickness of the capillary fringe varies along the water table even before swash-induced infiltrating seawater reaches the saturated portion of the beach at depth (Rows 2 and 3; $t = 1.5$ h). Heterogeneous capillarity also creates stronger gradients in moisture content and moisture hotspots and lowspots within the initially unsaturated zone. The moisture hotspots are located close to the beach surface and persist during long periods between individual swash events. The hotspots persist for ~ 2 hr after the swash zone recedes seaward as previously infiltrated seawater discharges through the lower saturated portion of the beach face ($t = 6.5$ and 7.5 h). Heterogeneity and associated moisture dynamics result in significant perturbation of the groundwater table as well. For example, compared to the homogeneous case, a low in the water table is observed when $t = 5.5$ h at location $x = 0.5$ and $x = 1.5$ m, which is most likely due to relatively low permeability that inhibits swash-induced infiltration (Figure 2).

Heterogeneity-induced capillary barriers create moisture hotspots in response to swash motions. For example, Figures 3a and 3b show a strong correlation between the moisture hotspots and heterogeneous capillarity at a later period during ebb tide ($t = 7.5$ h). It shows that moisture ratios (i.e. saturation) of 0.95 and 0.35 correspond strongly to configurations where a low K and high $1/\alpha$ layer is underlain by high K and low $1/\alpha$ layer. This is because as seawater drains from the unsaturated zone following a swash

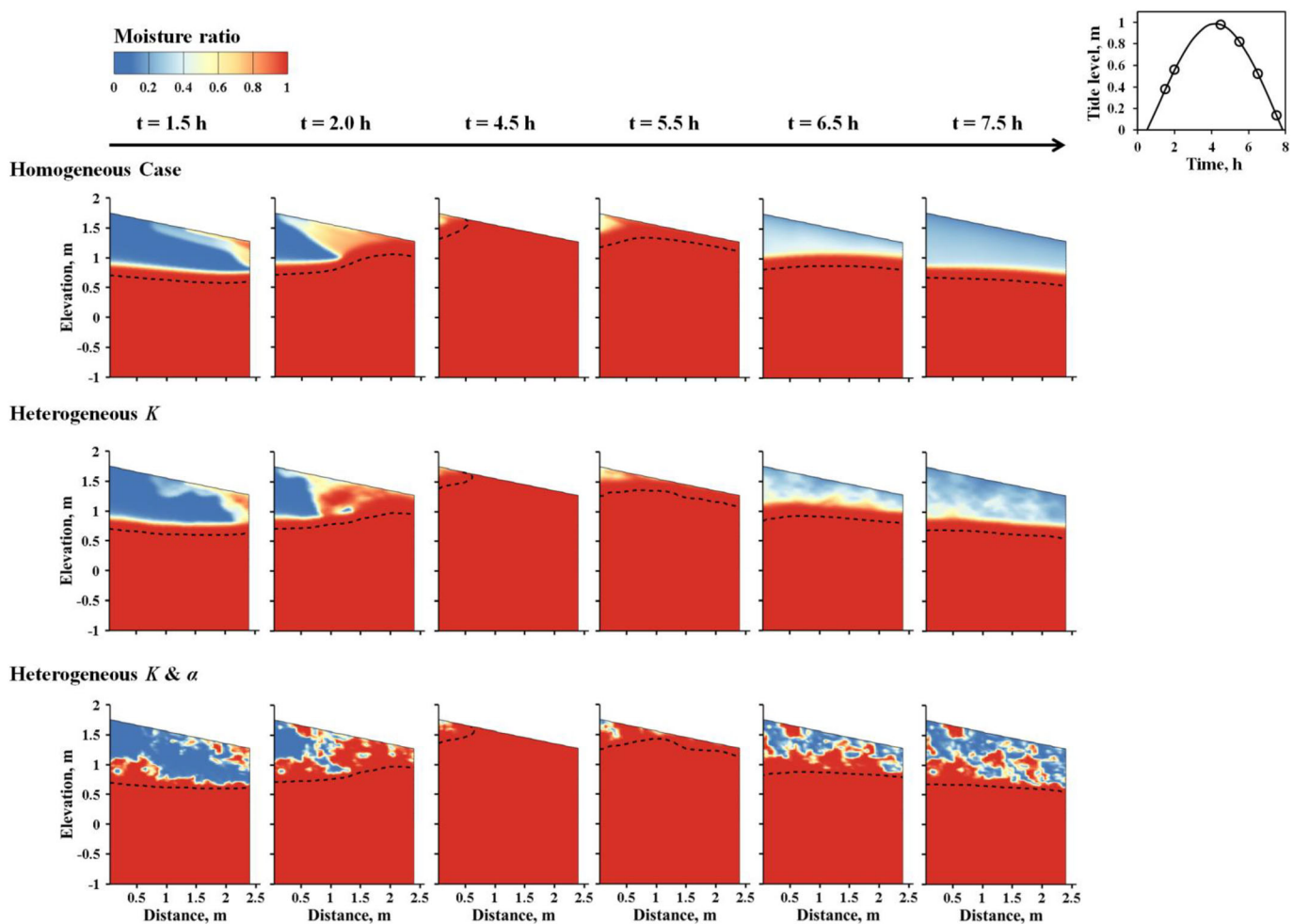


Figure 2. Simulated moisture ratio at different times within a tidal cycle for homogeneous and heterogeneous cases. The black-dashed line denotes groundwater table. Tidal fluctuations are provided in the rightmost panel where the time points selected for moisture contours are marked as circle symbols. The results for the heterogeneous cases correspond to the heterogeneous field illustrated in Figure 1.

event, the subsequent drop of pressure head causes a more rapid decrease in unsaturated hydraulic conductivity in the high K sediment than in low K areas. Drainage from low-permeability areas is therefore low because hydraulic conductivity in the surrounding high-permeability zones is extremely low. The resulting capillary tension limits flow from the low-permeability units to the surrounding high-permeability units, forming a capillary barrier to flow. In contrast, moisture hotspots (moisture ratio > 0.95) did not form in heterogeneous K . As shown in Figure 3c, the pockets of elevated moisture in heterogeneous K reached moisture ratios of only 0.35 within low-permeability zones (e.g., location at $x = 1.25$ m and $z = 1.1$ m). This is likely due to the homogeneous capillarity in heterogeneous K , which prevents capillary barriers from forming. Temporal evolution of the moisture content within single hotspot further demonstrates the role of capillarity on moisture dynamics beneath the swash zone for the homogeneous and heterogeneous cases (Figure 3d). The capillary barrier in heterogeneous K and α causes sediment within the hotspot to remain saturated even after the swash zone recedes seaward, while drainage from the sediment in heterogeneous K occurs during the same time period (Figure 3d; 6–8 h), decreasing the moisture content. The capillary barrier significantly affects the overall moisture level in the swash zone (Figure 4). Descriptive statistics of temporal variation of total moisture within the unsaturated portion of the swash zone consistently shows higher moisture level along with larger variance for heterogeneous K and α during the drainage period (between $t = 6$ and 7 h), as a result of the presence of the moisture hotspots.

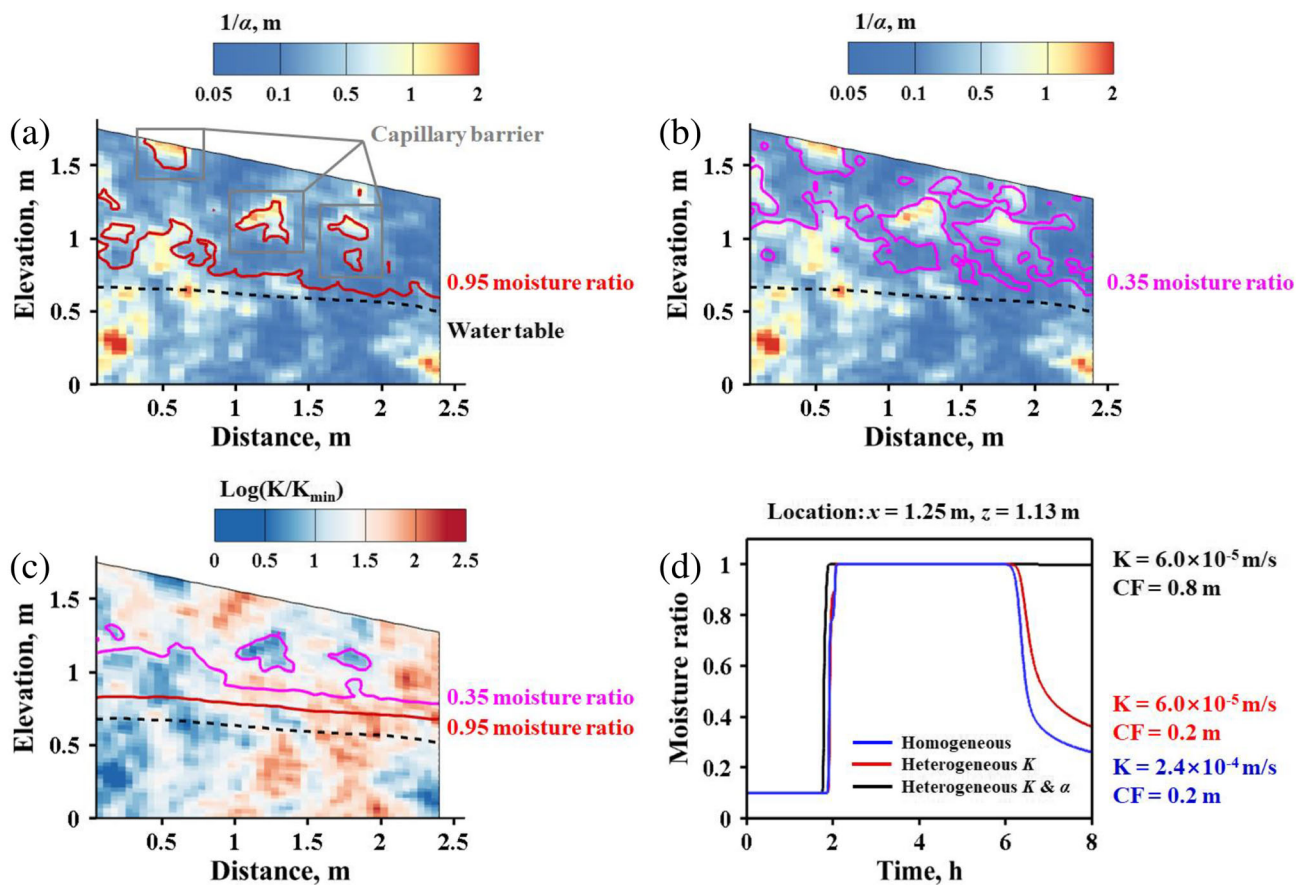


Figure 3. (a and b) Correlation between capillarity and a moisture ratio of 0.95 and 0.35 for heterogeneous K and α at later stage of ebb tide ($t = 7.5 \text{ h}$); (c) correlation between K and moisture ratio for heterogeneous K ; (d) temporal evolution of moisture ratio at $x = 1.25 \text{ m}$ and $z = 1.13 \text{ m}$ for heterogeneous and homogeneous cases. A value of $1/\alpha$ represents the theoretical height of capillary fringe as the porous media is unsaturated.

Heterogeneity significantly alters saturated and unsaturated flow velocities beneath the swash zone (Figure 5). In the homogeneous case (Row 1), swash-induced seawater infiltration forms a water table mound where water flows seaward on the sea side of the mound and landward on land side of the mound (e.g., $t = 2.0$ and 5.5 h). The resulting hydraulic gradient significantly elevates flow velocities along preferential flow paths in the saturated zone (e.g., $t = 1.5$ and 4.5 h). Once the tide and swash zone recede seaward of the model domain, percolating seawater continues to flow vertically through the unsaturated zone to the water table where it then flows seaward due to the large-scale terrestrial hydraulic gradient ($t = 6.5$ and 7.5 h). The water table mound also forms in both heterogeneous cases; however, velocity magnitudes are highly irregular over space owing to the heterogeneous hydraulic conductivity and capillarity. Localized areas of high pore-water velocities extend from the sand surface, through the unsaturated zone, and into the saturated zone, creating dendritic preferential flow paths in the higher K sediments (e.g., $t = 4.5$ and 5.5 h). The effects of heterogeneity in K and capillarity on groundwater flow rates and patterns are evident in Figure 5, Rows 2 and 3. In particular, flow paths are more tortuous in heterogeneous K and α compared to heterogeneous K as the tide recedes (e.g., $t = 6.5$ and 7.5 h). This is the result of the heterogeneity-induced capillary barriers in heterogeneous K and α , which forces percolating water to diverge around small-scale moisture hotspots in low-permeability zones. Heterogeneity greatly alters spatial pattern of seawater infiltration along the beach surface and the overall amount of seawater entering the aquifer in the swash zone (Figure 6). The descriptive statistics of the seawater infiltration for each heterogeneous case demonstrates a large discrepancy between its maximum and minimum values, indicating great spatial variability of swash-induced seawater infiltration caused by geologic heterogeneity (Figures 6a and 6b). Note that the infiltration is almost the same for the two heterogeneous cases. This is most likely because seawater

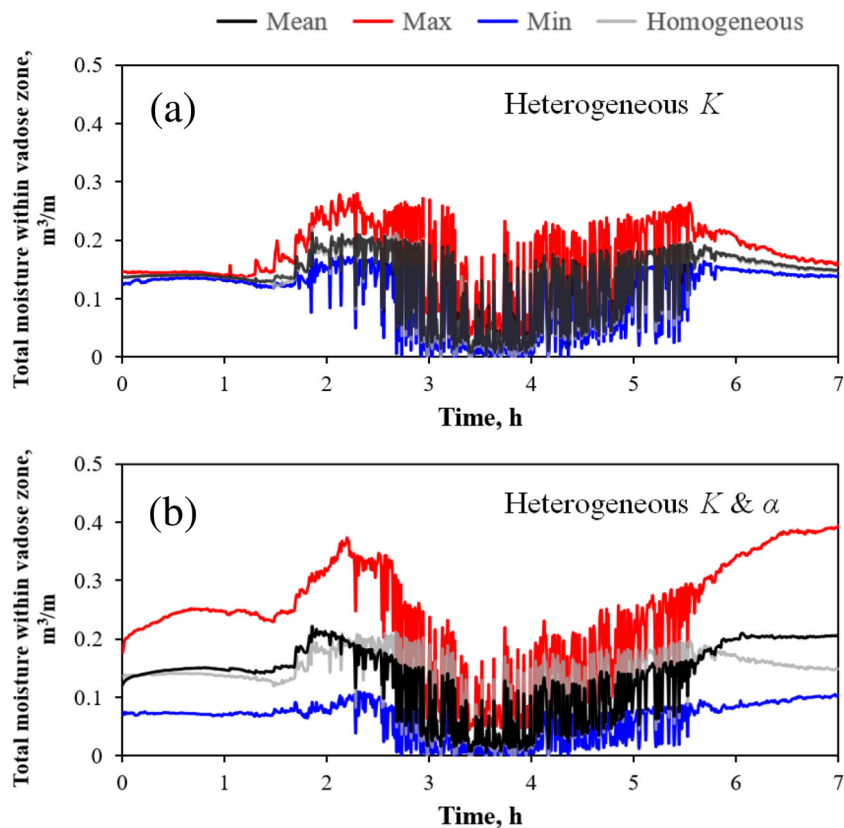


Figure 4. (a and b) Descriptive statistics of temporal variation of total moisture within vadose zone in response to swash motions for cases of heterogeneous K and heterogeneous K and α , respectively. Note that 30 realizations for each heterogeneous case were considered for statistical analysis.

infiltration likely saturates the swash zone surface, and therefore, capillary does not play a role. Figure 6c shows that the overall amount of seawater infiltration for heterogeneous cases on average is $3.2 \text{ m}^3/\text{m}$, which is $\sim 40\%$ higher than that of homogeneous case ($2.3 \text{ m}^3/\text{m}$).

Coupled with wave forcing, heterogeneity leads to complex flow topology within the swash zone (Figure 7). Contour plots of the Θ parameter show that for the homogeneous system, swash motions induce substantial strain-dominated flow regions (red/yellow colors) near the beach surface, while vorticity-dominated flow regions (blue color) form near the wet front of the infiltrating seawater, likely due to relatively high shear vorticity (Row 1, $t = 1.5\text{--}2.0 \text{ h}$). In contrast, local heterogeneity causes more complex spatial patterns in flow topology throughout the unsaturated and saturated zones. Heterogeneity creates pockets of vorticity-dominated flow regions. Instead of occurring near the wet front, these vorticity-dominated flow regions are embedded within strain-dominated flow regions during rising and high tide, indicating complex local-scale mixing. However, there are differences in the distribution of the vorticity- and strain-dominated regions between heterogeneous K and heterogeneous K and α during ebb tide (e.g., $t = 6.5$ and 7.5 h). The strain-dominated and vorticity-dominated flow regions extend to a higher elevation above the water table in heterogeneous K and α . For instance, at $t = 7.5 \text{ h}$ in heterogeneous K , the strain- and vorticity-dominated regions are uniformly $\sim 0.2 \text{ m}$ above the groundwater table across the profile. In contrast, in heterogeneous K and α , the strain- and vorticity-dominated regions reach as high as $\sim 0.7 \text{ m}$ above the water table. The difference in height of the strain- and vorticity-dominated regions above the water table is due to relatively higher moisture content and more tortuous preferential flow paths in heterogeneous K and α , where percolating pore water experiences greater deformation and rotation.

Figure 8 shows the temporal evolution of the total area of the strain-dominated flow region within the unsaturated zone. The area behaves similarly in both homogeneous and heterogeneous cases. The area increases when swash inundates the sand surface, reaching a first peak at $t = \sim 2 \text{ h}$, and then gradually decreases when

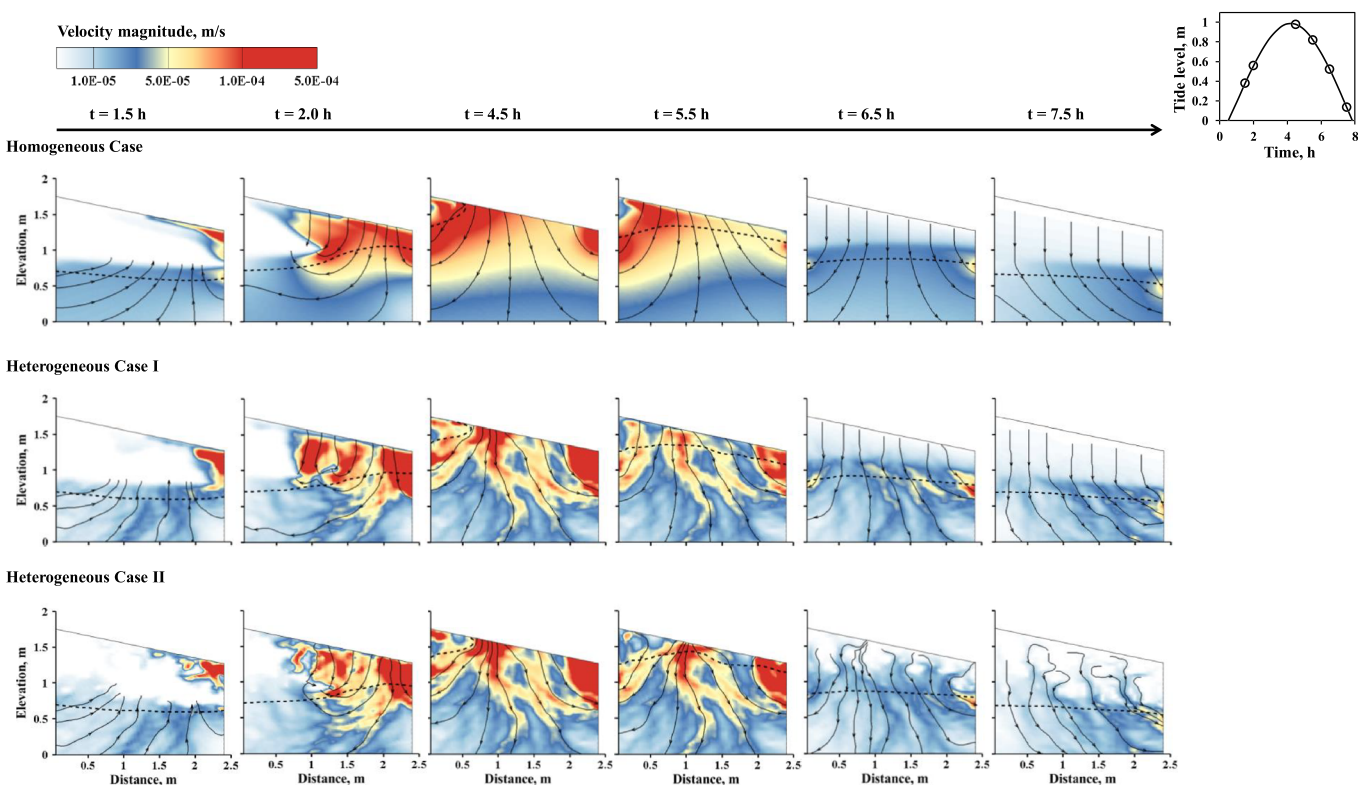


Figure 5. Simulated flow velocity along with transient streamlines of pore water flow within the swash zone for homogeneous and heterogeneous cases at different times within a tidal cycle. The black-dashed line denotes the groundwater table. The results for heterogeneous cases correspond to the heterogeneous field illustrated in Figure 1.

swash events become more frequent (Figures 8a and 8b). The area rises again when the swash zone moves seaward and then reaches a second peak at $t = \sim 6$ h after which the area gradually decreases. The increase in the area of the strain-dominated region near the beginning of the simulation can be attributed to the large quantity of seawater that infiltrates into initially dry sediment. The decrease in area ($t = 2\text{--}3.5$ h) is the result of a rising water table from continuous seawater infiltration that reduces the thickness of the unsaturated zone, leading to the decrease in the area available for strain-dominated unsaturated flow. As the swash zone begins to shift seaward at $t = 3.5$ h, the water table slowly declines, and the unsaturated zone and the total strain-dominated area expand downward.

The strain-dominated area oscillates rapidly in response to individual waves; the area increases when pressure head (i.e., water table) declines and decreases when pressure head rises during swash inundation (Figures 8d and 8e). The strain-dominated area in the heterogeneous cases is smaller than the homogeneous case when the groundwater table approaches the sand surface (Figure 8b; between $t = 2$ and 6 h). This is likely the result of the large quantity of seawater that infiltrates the beach surface during this time period. The tortuous vertical flowpaths in the heterogeneous models create both strain-dominated and vorticity-dominated flows, which to some extent limits the extent of the strain-dominated flow regions compared to the homogeneous system. However, the opposite occurs during ebb tide ($t = > 6$ h) when the swash zone moves seaward of the model domain and the total strain-dominated area is larger for the heterogeneous cases compared to the homogeneous case. This behavior is likely the result of the relative importance of external wave forcing. In the homogeneous system, fluid that is deformed along unsaturated flow paths is mainly driven by external wave forcing acting on the beach, and thus, the area of the strain-dominated region drops fastest. In contrast, flow deformation in the heterogeneous systems is attributed to both external wave forcing and internal local heterogeneity; hence, the strain-dominated area is larger during the later stages of ebb tide.

The total vorticity-dominated area within the unsaturated zone follows a similar temporal pattern to that of the strain-dominated regions (Figures 8c and 8f). However, the vorticity-dominated area is always

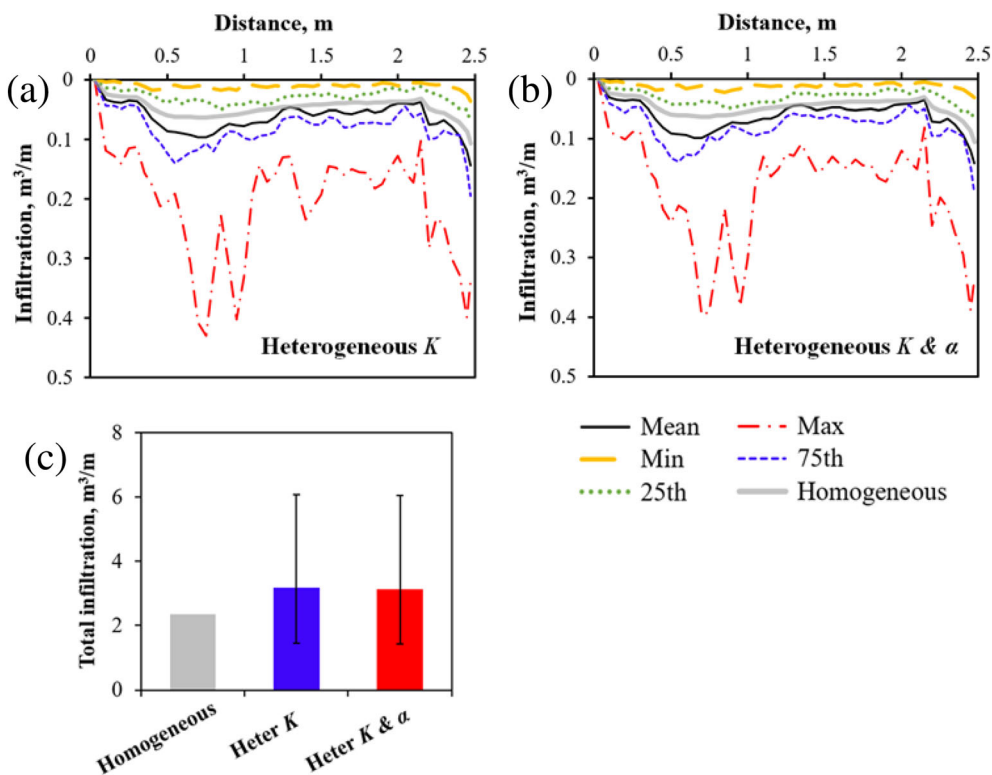


Figure 6. (a and b) Spatial distribution of wave-induced seawater infiltration along the beach surface for cases of heterogeneous K and heterogeneous K and α , respectively. (c) Total seawater infiltration along the beach surface during the simulated swash period for homogeneous and heterogeneous cases. The solid columns represent the mean, and whiskers represent the maximum and minimum infiltration rate from the 30 realizations.

larger in the heterogeneous cases, which is as expected due to the more torturous preferential flow paths. Additionally, the size of the fluctuations in area during the period with frequent swash inundation ($t = 2.5\text{--}5.5$ h) is largest in heterogeneous K (Figure 8c). The difference in the size of the fluctuations is the result of the contrasting responses of unsaturated hydraulic conductivity to changes in moisture content. As pressure throughout the unsaturated zone decreases following a swash event, areas with fine-grained sediment for heterogeneous K and α remain saturated for a long duration because of capillary forces. The adjacent coarse-grained sediments drain rapidly due to larger pores, which lower the K value in those sediments. This lowers the contrast in K between the fine-grained and coarse-grained sediments, thus reducing the velocity gradient and corresponding shear and curvature vorticity, leading to a smaller vorticity-dominated area. Ensemble-averaged statistics of 30 geologic realizations indicate that the strain-dominated and vorticity-dominated flow regions are larger in the heterogeneous cases than in the homogeneous case when the swash zone is seaward of the model domain ($t = 6\text{--}7$ h), indicating that the effects of heterogeneity are most pronounced during falling tide (Figure 9).

Heterogeneity causes complex mixing of pore water in response to swash motions (Figure 10). The dilution index (E) of groundwater in the homogeneous case is higher near the beach surface when the swash zone first approaches the model domain ($t = 2.0$ h). Note that the dilution index has been normalized by the maximal value among heterogeneous and homogeneous systems, therefore varying between 0 and 1. Relatively high E expands downward and landward as the unsaturated zone becomes saturated from swash infiltration ($t = 2.0, 4.5$, and 5.5 h) and drops near the sand surface during ebb tide ($t = 6.5$ and 7.5 h). In contrast, heterogeneity greatly enhances the magnitude and the spatial variability of E . It creates significant hot and low spots of E throughout the tidal cycle. The importance of capillarity on E is also evident. For heterogeneous K and α , as swash motions recede during ebb tide ($t = 6.5\text{--}7.5$ h), zones of relatively high E expand and branch upward above the water table (Figure 10; Row 3). These high-dilution branches occur primarily in low K zones during later stages of ebb tide. This is because relatively high capillarity (i.e., $1/\alpha$) in low K zones

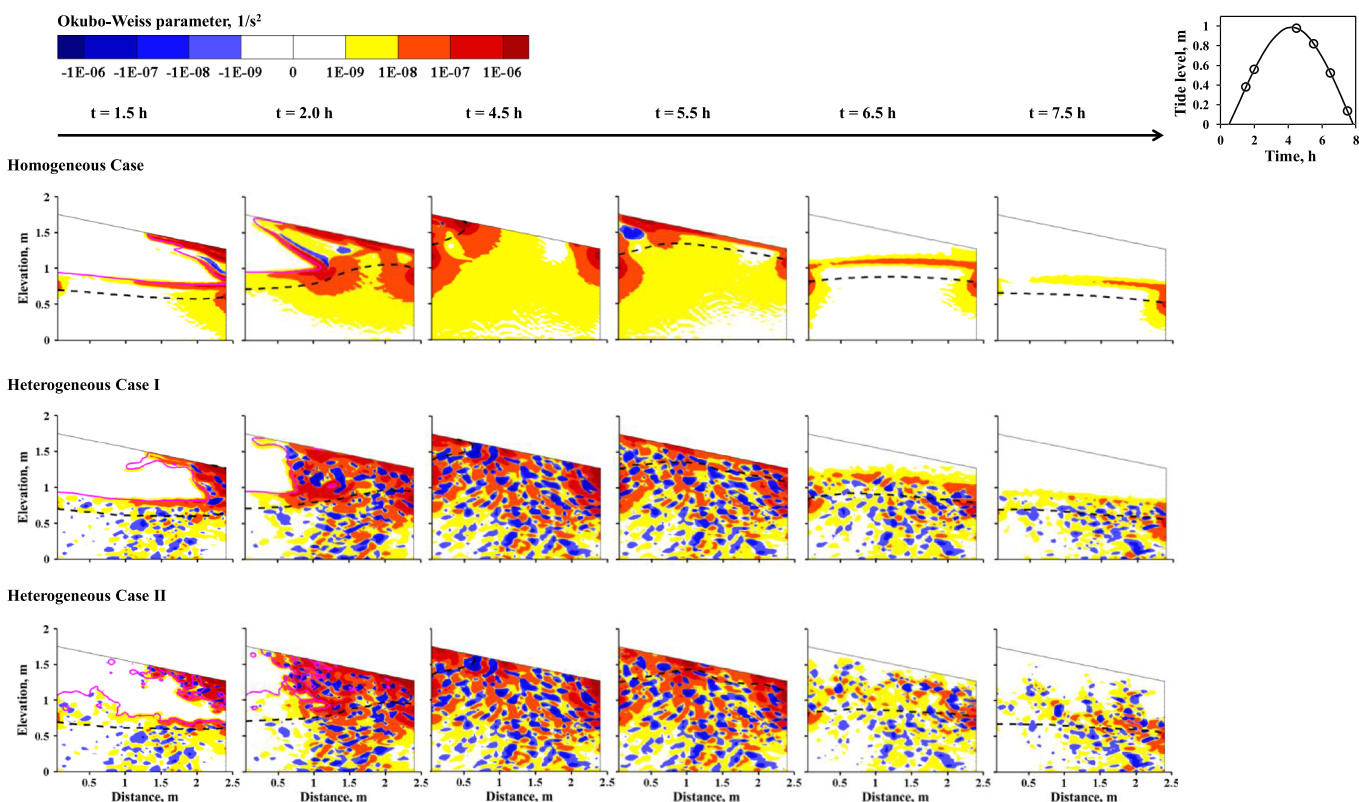


Figure 7. Contour of the Okubo-Weiss parameter for homogeneous and heterogeneous cases at different times within a tidal cycle. The black-dashed line denotes the groundwater table. The wetting front (moisture ratio of 0.3) is marked as solid magenta line at time $t = 1.5$ and 2 h. The results for heterogeneous cases correspond to the heterogeneous field illustrated in Figure 1.

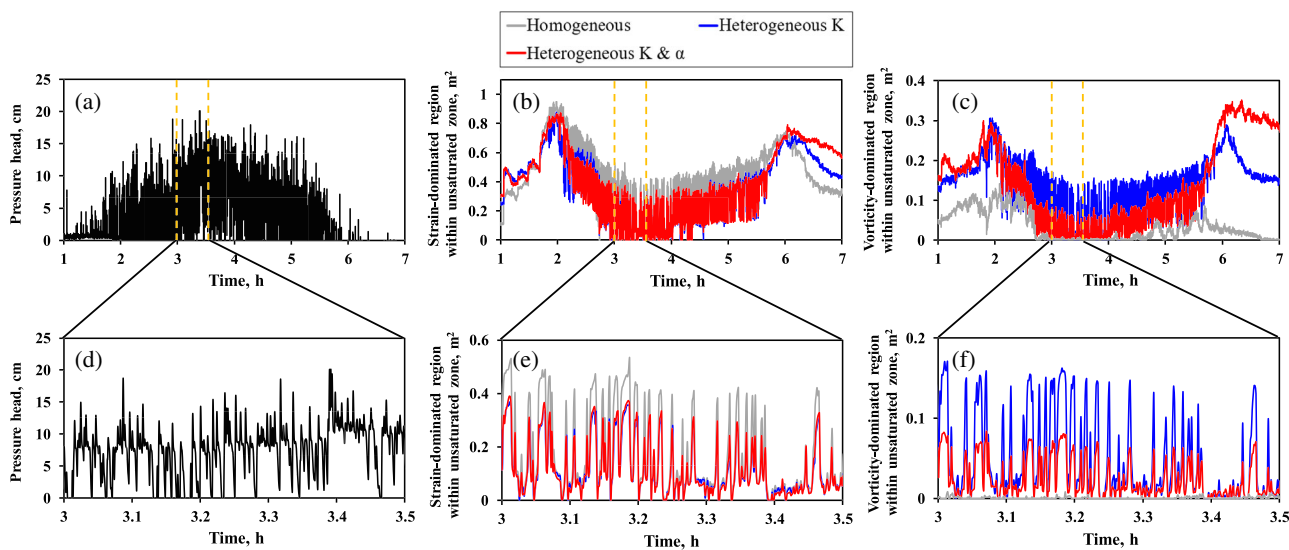


Figure 8. (a) Wave-induced pressure oscillations at the surface boundary; (b and c) temporal evolution of the total area of the strain-dominated and vorticity-dominated flow area within the unsaturated zone, respectively. Figures 8a–8c are zoomed in at a time period from $t = 3$ – 3.5 h and shown in Figures 8d–8f.

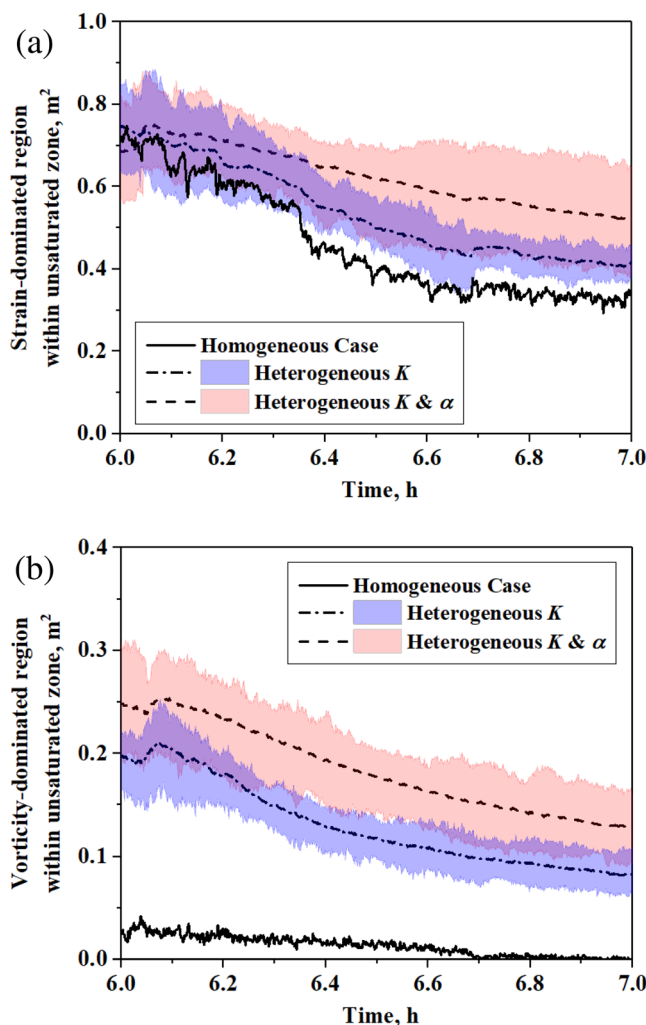


Figure 9. Temporal evolution of the areal extent of strain-dominated and vorticity-dominated flow regions in response to wave motions between $t = 6$ and 7 h when the largest discrepancy is observed among homogeneous and heterogeneous cases, taking into account 30 realizations for each homogeneous and heterogeneous cases. The lines and shading represent the mean and range between the minimum and maximum of the total area among the realizations, respectively.

tion at each tidal stage in response to swash motions. Within the strain-dominated flow regions, stretching and deformation of fluid filaments result in a relatively high-dilution rate of solutes (e.g., dissolved oxygen and nutrients), promoting mineralization of organic matter; in contrast, within the vorticity-dominated flow regions, rotation of fluid filaments leads to less dilution of solutes and likely induces oxygen deficit and nutrient buildup in the sediments. Differences in magnitude and spatial variability of seawater infiltration between heterogeneous and homogeneous cases indicate an important role of geologic heterogeneity in geochemical budget and zonation within marine sediments. Biogeochemical hotspots in coastal marine environments have been observed in numerous field studies (Kim et al., 2019; Schutte et al., 2015, 2018). The hotspots of mixing simulated in this paper likely intensify mixing-dependent geochemical reactivity, which might provide plausible interpretations for these field observations. Differences in magnitudes and paths of the unsaturated flow in response to swash motions between two heterogeneous cases also highlight the importance of considering both heterogeneous K and capillarity when modeling unsaturated flow and transport processes beneath the swash zone. The complex flow and moisture dynamics in the swash zone as shown in this study also suggest that it is important to consider dimensionality in such investigations. For example, due to

allows unsaturated hydraulic conductivity to remain relatively high even after a large drop of pore-water pressure potential (e.g., 0.4 m), while in high K zones, hydraulic conductivity sharply decreases with the drop of pressure potential. The resulting large velocity contrast, therefore, engenders the upward branching of areas with elevated E .

Figure 11 shows the probability of relatively high E (>0.1) for heterogeneous K and K and α at $t = 2.0$ and 7.5 h accounting for all geologic realizations. The results show that the probability of relatively high dilution during rising tide is highest in the shallow beach (~1-m depth) for both heterogeneous cases (Figures 11a and 11b), with greater spatial variability for heterogeneous K and α . This is also the case during ebb tide (Figures 11c and 11d). The total area of different probability ranges also differs between two heterogeneous cases (Figures 11e and 11f). The area of lower probability zones ($<70\%$) is consistently higher for heterogeneous K and α , indicating that heterogeneous capillarity results in significant spatial variability in the dilution rate. The difference in the probability of the high-dilution index ($>70\%$) between the two heterogeneous cases further indicates that it is important to consider capillarity when modeling groundwater flow in the swash zone.

4. Discussion

Our results reveal complex subsurface flow pathways and highly variable local-scale mixing in response to swash motions in the presence of heterogeneity. Coastal sedimentary environments have been identified as a biogeochemical zone where a significant amount of organic matter is trapped and decomposed (Bacon et al., 1994; Kim et al., 2017; McLachlan et al., 1985). Seawater infiltration is a major source of dissolved oxygen that enhances sedimentary respiration and mineralization reactions (Anschutz et al., 2009; Geng et al., 2015; Santos et al., 2009). For example, Anschutz et al. (2009) observed significant depletion of dissolved oxygen and increase in dissolved nitrate and dissolved inorganic phosphorus within near-surface beach sediments, indicating the respiration of organic matter occurs as soon as seawater enters the sediment. In this paper, we delineate for the first time swash zone flow topology using the Okubo-Weiss parameter and reveal that percolating seawater moving through unsaturated sediments experiences significant local-scale deformation beneath the swash zone. Analysis of dilution indices further indicate complex mixing processes in beach aquifers as spatial-temporal variability of local-scale flow topology creates significant hot and low spots of the rate of the dilution.

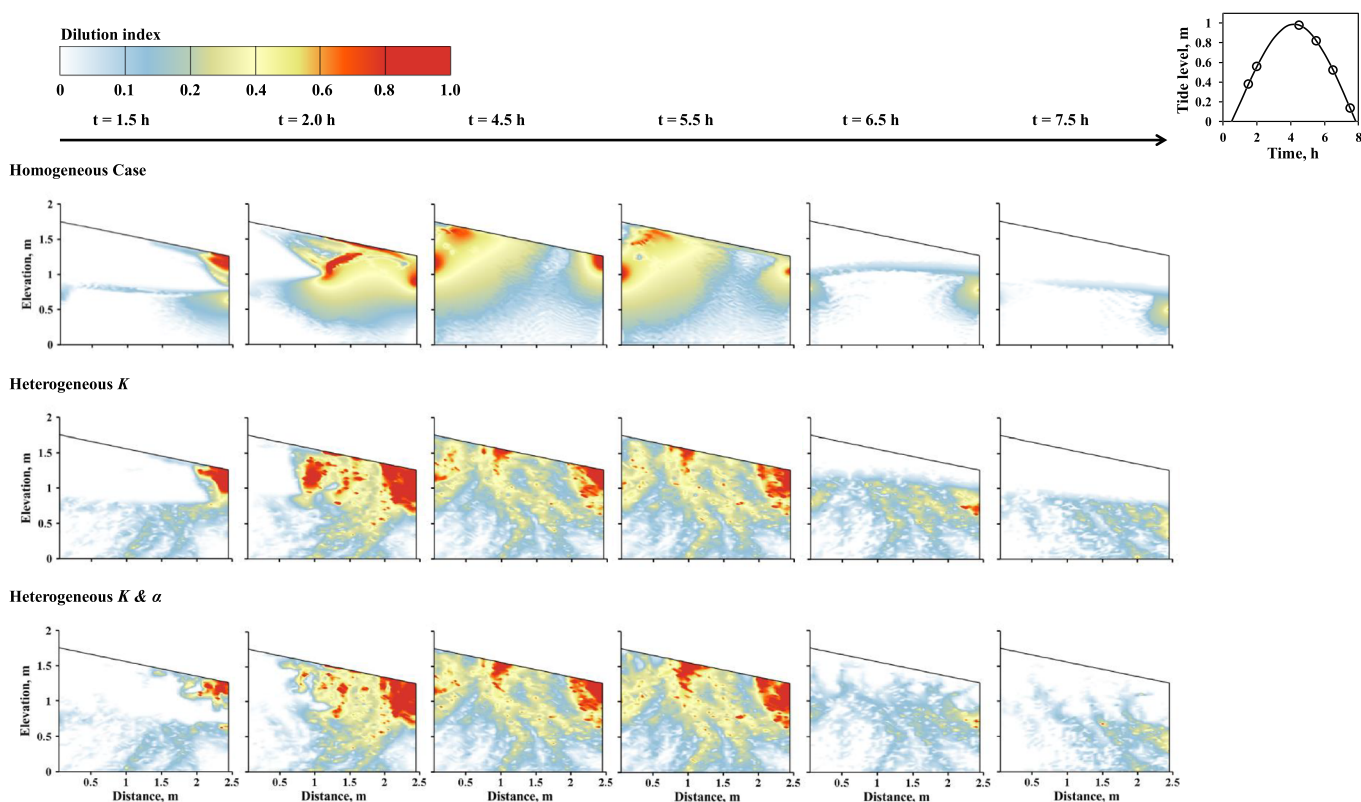


Figure 10. Contour of dilution index for the homogeneous and heterogeneous cases at different times within a tidal cycle. The dilution index is calculated for each cell for 60 s (~6–7 swash cycles) (Equation 12) and normalized by the maximum value among heterogeneous and homogeneous systems, therefore varying between 0 and 1. The results for heterogeneous cases correspond to the heterogeneous field illustrated in Figure 1.

heterogeneity, 3-D groundwater flow can exhibit more complex flow patterns with helical and intertwining streamlines (Bakker & Hemker, 2004; Chiogna et al., 2014; Cirpka et al., 2015), which could greatly increase transverse mixing in aquifers, and needs to be taken into account in future studies.

Our study highlights the importance of geologic heterogeneity in swash zone moisture and flow dynamics. Numerous studies have been conducted to investigate nearshore groundwater dynamics in response to wave forcing, though the primary focus has been on homogeneous beach systems (Boufadel et al., 2007; Geng et al., 2014, 2017; Geng & Boufadel, 2015; Heiss et al., 2014, 2015; Malott et al., 2017; Robinson et al., 2014; Xin et al., 2010). In this paper, we illustrate for the first time that heterogeneity increases the spatial variability of moisture content in the swash zone in response to individual waves and show that heterogeneous capillarity creates moisture hotspots beneath the swash zone. Due to the formation of capillary barriers, the capillary tension allows those moisture hotspots to persist over tidal cycles, which is likely to have implications for microbial community habitat and associated biogeochemical processes in heterogeneous nearshore aquifers. For example, in marine sediments, moisture content can be a critical factor affecting N mineralization by regulating osmotic potential, redox potential, and water availability (Jia et al., 2019; Tian et al., 2010; Yin et al., 2019). Jia et al. (2019) demonstrated that rates of N mineralization and nitrification increase with an increase in salinity at saturated conditions, while reaction rates did not change with salinity at moderate moisture levels (50% saturation). Further, spatially heterogeneous moisture content can influence the composition, motility, and survival of microorganisms responsible for biodegradation of contaminants (Yadav & Hassanzadeh, 2011). Contaminant transport is also likely to be affected, as the presence of capillary barriers can result in entrapment of dense nonaqueous phase liquids (DNAPLs) in heterogeneous aquifer formations (Bradford et al., 1998). In coastal marine systems, the supralittoral and sublittoral zones have been recognized as most vulnerable to various sea-derived contaminants such as oil spills (Boufadel et al., 2014; Geng et al., 2015, 2016; Huettel et al., 2018; Shin et al., 2019). Studies revealed that subsurface oil contamination due to offshore spills can persist within beach sediments for years to decades (Bernabeu

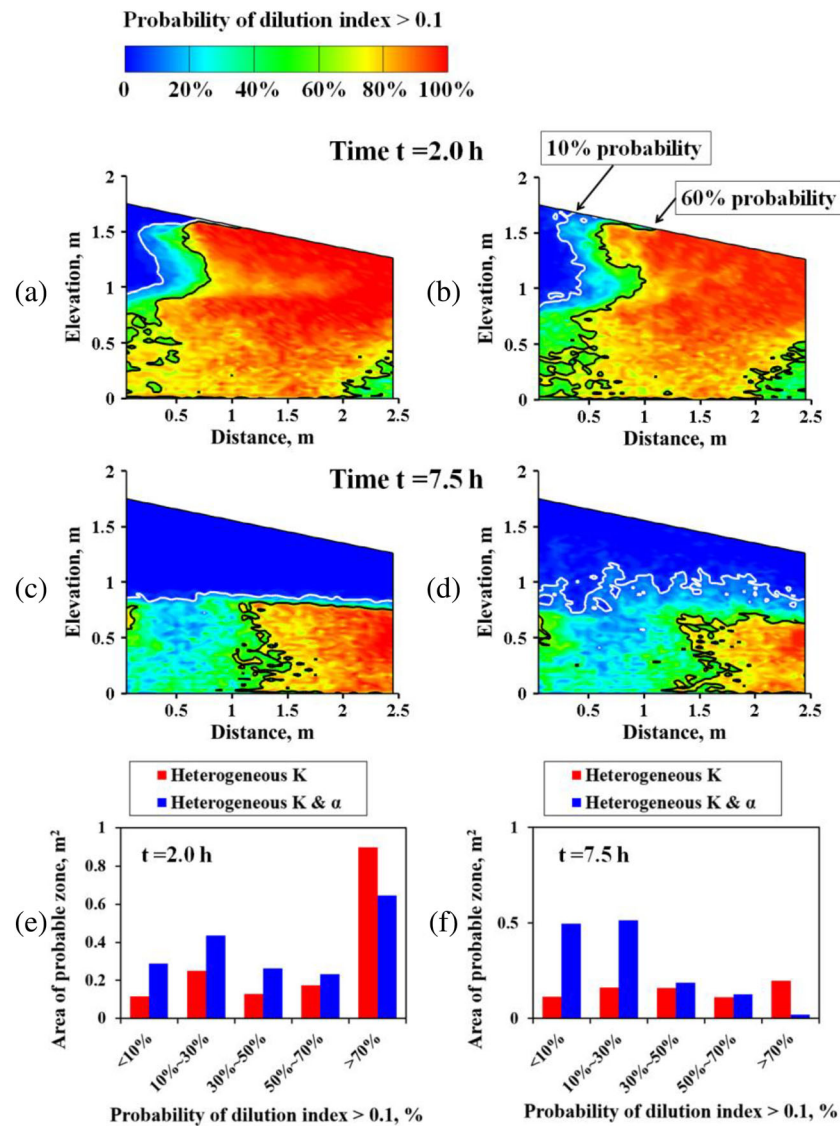


Figure 11. Probability of dilution index > 0.1 at (a and b) $t = 2.0\text{ h}$ and (c and d) $t = 7.5\text{ h}$ for heterogeneous K and K and α , respectively. Area of different probability zones of dilution index > 0.1 for heterogeneous cases K and K and α at (e) $t = 1.5\text{ h}$ and (f) $t = 7.5\text{ h}$. The probability is calculated using Equation 11, considering all 30 realizations.

et al., 2009; Boufadel et al., 2010), and degradation of oil contaminants within the sediments is mainly mediated by microorganisms whose activities are affected by various environmental factors such as salinity, moisture, and nutrient and oxygen conditions (Atlas & Hazen, 2011; Boufadel et al., 2016; Kostka et al., 2011). Thus, our results suggest that the spatially heterogeneous moisture distributions and associated moisture hotspots shown in the present study can have substantially lasting effects on the composition, motility, and survival of microorganisms responsible for biodegradation of oil residuals trapped within the beach sediments. Geng et al. (2020a) quantified the flow topology in porous media from a 3-D perspective using Q criterion (Haller, 2015) (i.e., 3-D form of Okubo-Weiss parameter). Their results found that heterogeneity-induced coherent Lagrangian vortices exhibit scale-invariant features in both multifractal and stationary heterogeneous permeability fields, implying that those vortex structures could be widely present in groundwater systems with no characteristic scales. That indicates that the vortex structures identified in this paper within coastal aquifers could be potentially measured in practice over a wide range of spatial scales.

5. Conclusion

A density-dependent, variably saturated groundwater flow model was used with heterogeneous K fields in a Monte Carlo framework to investigate moisture and flow dynamics beneath the swash zone. Our results show that heterogeneous capillarity greatly affects tempo-spatial evolution of swash zone moisture content. In models with heterogeneous capillarity, the height of the capillary fringe varied across the water table and moisture hotspots formed in the unsaturated zone due to capillary barriers between high and low K sediment. Heterogeneity significantly alters the magnitude and spatial distribution of seawater infiltration along the swash surface. Heterogeneous capillarity resulted in highly tortuous flow paths and altered the magnitude of flow rates from the sand surface to the water table. Simulation results suggest that beaches host complex tempo-spatial patterns in subsurface flow topology in response to swash motions. In particular, compared to the homogeneous system, heterogeneity in both K and capillarity generates significant strain-dominated and vorticity-dominated flow regions beneath the swash zone as the tide and swash zone retreat seaward during falling tide, which affects local-scale mixing dynamics. Heterogeneous porous media creates complex mixing and flow patterns due to the formation of preferential flow paths in the unsaturated zone. Our findings reveal important influences of geologic heterogeneity on swash zone moisture and flow dynamics and indicate that geologic heterogeneity in both K and capillarity is an important factor when investigating groundwater flow and transport processes in saturated and unsaturated sediments beneath the swash zone. Geologic heterogeneity has been ubiquitously observed at varying degrees in coastal aquifers and biogeochemical processing of land- and sea-derived reactive solutes within these systems is enhanced where mixing is intensified. Therefore, the numerical schemes and associated findings presented herein are likely to have strong implications for understanding microbial habitats in intertidal sediments and for predicting chemical reactivity in shallow coastal aquifers.

Data Availability Statement

Data are published with CUAHSI Hydroshare database <https://doi.org/10.4211/hs.52c1794108d94e00af3ea43badf14965>.

Acknowledgments

We would like to thank Yu Wang for improving figures and Zijun Ou and Bing Yu for creating an online accessible database, storing all the simulation files and field data presented in this paper. This work was supported in part by the Multi Partner Research Initiative project Oil Translocation from the Department of Fisheries and Oceans, Canada and by the US National Science Foundation (EAR1151733). However, it does not necessarily reflect the views of the funding entity; no official endorsement should be inferred.

References

- Adams, E. E., & Gelhar, L. W. (1992). Field study of dispersion in a heterogeneous aquifer: 2. Spatial moments analysis. *Water Resources Research*, 28(12), 3293–3307. <https://doi.org/10.1029/92WR01757>
- Anschutz, P., Smith, T., Mouret, A., Debordé, J., Bujan, S., Poirier, D., & Leroart, P. (2009). Tidal sands as biogeochemical reactors. *Estuarine, Coastal and Shelf Science*, 84(1), 84–90.
- Anwar, N., Robinson, C., & Barry, D. A. (2014). Influence of tides and waves on the fate of nutrients in a nearshore aquifer: Numerical simulations. *Advances in Water Resources*, 73, 203–213.
- Atherton, R. J., Baird, A. J., & Wiggs, G. F. (2001). Inter-tidal dynamics of surface moisture content on a meso-tidal beach. *Journal of Coastal Research*, 482–489.
- Atlas, R. M., & Hazen, T. C. (2011). Oil biodegradation and bioremediation: A tale of the two worst spills in US history. *Environmental Science & Technology*, 45(16), 6709–6715. <https://doi.org/10.1021/es2013227>
- Bacon, M., Belastock, R. A., & Bothner, M. H. (1994). 210Pb balance and implications for particle transport on the continental shelf, US Middle Atlantic Bight. *Deep Sea Research Part II: Topical Studies in Oceanography*, 41(2–3), 511–535.
- Bak, P., & Creutz, M. (1993). *Fractals and Disordered Systems*. Berlin Heidelberg: Springer-Verlag.
- Bakhtyar, R., Brovelli, A., Barry, D. A., & Li, L. (2011). Wave-induced water table fluctuations, sediment transport and beach profile change: Modeling and comparison with large-scale laboratory experiments. *Coastal Engineering*, 58(1), 103–118.
- Bakker, M., & Hemker, K. (2004). Analytic solutions for groundwater whirls in box-shaped, layered anisotropic aquifers. *Advances in Water Resources*, 27(11), 1075–1086.
- Bernabeu, A. M., Rey, D., Rubio, B. N., Vilas, F., Domínguez, C., Bayona, J. M., & Albaiges, J. (2009). Assessment of cleanup needs of oiled sandy beaches: Lessons from the Prestige oil spill. *Environmental Science & Technology*, 43(7), 2470–2475. <https://doi.org/10.1021/es803209h>
- Boehm, A. B., Paytan, A., Shellenbarger, G. G., & Davis, K. A. (2006). Composition and flux of groundwater from a California beach aquifer: Implications for nutrient supply to the surf zone. *Continental Shelf Research*, 26(2), 269–282.
- Boufadel, M. C., Abdollahi-Nasab, A., Geng, X., Galt, J., & Torlapati, J. (2014). Simulation of the landfall of the Deepwater Horizon oil on the shorelines of the Gulf of Mexico. *Environmental Science & Technology*, 48(16), 9496–9505. <https://doi.org/10.1021/es5012862>
- Boufadel, M. C., Geng, X., & Short, J. (2016). Bioremediation of the Exxon Valdez oil in Prince William sound beaches. *Marine Pollution Bulletin*, 113(1–2), 156–164. <https://doi.org/10.1016/j.marpolbul.2016.08.086>
- Boufadel, M. C., Li, H., Suidan, M. T., & Venosa, A. D. (2007). Tracer studies in a laboratory beach subjected to waves. *Journal of Environmental Engineering*, 133(7), 722–732.
- Boufadel, M. C., Lu, S., Molz, F. J., & Lavallee, D. (2000). Multifractal scaling of the intrinsic permeability. *Water Resources Research*, 36(11), 3211–3222.
- Boufadel, M. C., Sharifi, Y., Van Aken, B., Wrenn, B. A., & Lee, K. (2010). Nutrient and oxygen concentrations within the sediments of an Alaskan beach polluted with the Exxon Valdez oil spill. *Environmental Science & Technology*, 44(19), 7418–7424. <https://doi.org/10.1021/es102046n>

- Boufadel, M. C., Suidan, M. T., & Venosa, A. D. (1999). A numerical model for density-and-viscosity-dependent flows in two-dimensional variably-saturated porous media. *Journal of Contaminant Hydrology*, 36, 1–20.
- Bradford, S. A., Abriola, L. M., & Rathfelder, K. M. (1998). Flow and entrainment of dense nonaqueous phase liquids in physically and chemically heterogeneous aquifer formations. *Advances in Water Resources*, 22(2), 117–132.
- Brown, K. I., & Boehm, A. B. (2016). Transport of fecal indicators from beach sand to the surf zone by recirculating seawater: Laboratory experiments and numerical modeling. *Environmental Science & Technology*, 50(23), 12,840–12,847.
- Cartwright, N., Nielsen, P., & Jessen, O. Z. (2002). Swash zone and near-shore watertable dynamics. In *Proceedings of the 28th International Conference on Coastal Engineering, Cardiff, Wales* (pp. 1006–1015). New York: World Scientific.
- Cassman, K., & Munns, D. (1980). Nitrogen mineralization as affected by soil moisture, temperature, and depth. *Soil Science Society of America Journal*, 44(6), 1233–1237.
- Chiogna, G., Rolle, M., Bellin, A., & Cirpka, O. A. (2014). Helicity and flow topology in three-dimensional anisotropic porous media. *Advances in Water Resources*, 73, 134–143.
- Cirpka, O. A., Chiogna, G., Rolle, M., & Bellin, A. (2015). Transverse mixing in three-dimensional nonstationary anisotropic heterogeneous porous media. *Water Resources Research*, 51, 241–260. <https://doi.org/10.1002/2014WR015331>
- Dagan, G. (2012). *Flow and transport in porous formations*. New York: Springer Science & Business Media.
- de Alava, A., & Defeo, O. (1991). Distributional pattern and population dynamics of *Exciorolana armata* (Isopoda: Cirolanidae) in a Uruguayan sandy beach. *Estuarine, Coastal and Shelf Science*, 33(5), 433–444.
- de Barros, F. P., Dentz, M., Koch, J., & Nowak, W. (2012). Flow topology and scalar mixing in spatially heterogeneous flow fields. *Geophysical Research Letters*, 39, L08404. <https://doi.org/10.1029/2012GL051302>
- Defeo, O., & McLachlan, A. (2005). Patterns, processes and regulatory mechanisms in sandy beach macrofauna: A multi-scale analysis. *Marine Ecology Progress Series*, 295, 1–20.
- Dentz, M., de Barros, F., Le Borgne, T., & Lester, D. (2018). Evolution of solute blobs in heterogeneous porous media. *Journal of Fluid Mechanics*, 853, 621–646.
- Dentz, M., Le Borgne, T., Englert, A., & Bijeljic, B. (2011). Mixing, spreading and reaction in heterogeneous media: A brief review. *Journal of Contaminant Hydrology*, 120, 1–17.
- Gelhar, L. W. (1993). *Stochastic subsurface hydrology*. Englewood Cliffs, New Jersey: Prentice-Hall.
- Geng, X., & Boufadel, M. C. (2015). Numerical study of solute transport in shallow beach aquifers subjected to waves and tides. *Journal of Geophysical Research: Oceans*, 120, 1409–1428. <https://doi.org/10.1002/2014JC010539>
- Geng, X., Boufadel, M. C., Lee, K., Abrams, S., & Suidan, M. (2015). Biodegradation of subsurface oil in a tidally influenced sand beach: Impact of hydraulics and interaction with pore water chemistry. *Water Resources Research*, 51, 3193–3218. <https://doi.org/10.1002/2014WR016870>
- Geng, X., Boufadel, M. C., Lee, K., & An, C. (2020a). Characterization of pore water flow in 3D heterogeneous permeability fields. *Geophysical Research Letters*, 47, e2019GL086879. <https://doi.org/10.1029/2019GL086879>
- Geng, X., Boufadel, M. C., Rajaram, H., Cui, F., Lee, K., & An, C. (2020b). Numerical study of solute transport in heterogeneous beach aquifers subjected to tides. *Water Resources Research*, 56, e2019WR026430. <https://doi.org/10.1029/2019WR026430>
- Geng, X., Boufadel, M. C., Xia, Y., Li, H., Zhao, L., Jackson, N. L., & Miller, R. S. (2014). Numerical study of wave effects on groundwater flow and solute transport in a laboratory beach. *Journal of Contaminant Hydrology*, 165, 37–52. <https://doi.org/10.1016/j.jconhyd.2014.07.001>
- Geng, X., Heiss, J. W., Michael, H. A., & Boufadel, M. C. (2017). Subsurface flow and moisture dynamics in response to swash motions: Effects of beach hydraulic conductivity and capillarity. *Water Resources Research*, 53, 10,317–10,335. <https://doi.org/10.1002/2017WR021248>
- Geng, X., & Michael, H. A. (2020). Preferential flow enhances pumping-induced saltwater intrusion in volcanic aquifers. *Water Resources Research*, 56, e2019WR026390. <https://doi.org/10.1029/2019WR026390>
- Geng, X., Pan, Z., Boufadel, M. C., Ozgokmen, T., Lee, K., & Zhao, L. (2016). Simulation of oil bioremediation in a tidally influenced beach: Spatiotemporal evolution of nutrient and dissolved oxygen. *Journal of Geophysical Research: Oceans*, 121, 2385–2404. <https://doi.org/10.1002/2015JC011221>
- Gray, C. A., Johnson, D. D., Reynolds, D., & Rotherham, D. (2014). Development of rapid sampling procedures for an exploited bivalve in the swash zone on exposed ocean beaches. *Fisheries Research*, 154, 205–212.
- Guntiñas, M. E., Leirós, M., Trasar-Cepeda, C., & Gil-Sotres, F. (2012). Effects of moisture and temperature on net soil nitrogen mineralization: A laboratory study. *European Journal of Soil Biology*, 48, 73–80.
- Haller, G. (2015). Lagrangian coherent structures. *Annual Review of Fluid Mechanics*, 47, 137–162.
- Heiss, J., Michael, H., & Koneshlo, M. (2020). Denitrification hotspots in intertidal mixing zones linked to geologic heterogeneity. *Environmental Research Letters*, 15(8), 084015. <https://doi.org/10.1088/1748-9326/ab90a6>
- Heiss, J. W., Michael, H. A., & Puleo, J. A. (2020). Groundwater-surface water exchange in the intertidal zone detected by hydrologic and coastal oceanographic measurements. *Hydrological Processes*. <https://doi.org/10.1002/hyp.13825>
- Heiss, J. W., Post, V. E., Laattoe, T., Russoniello, C. J., & Michael, H. A. (2017). Physical controls on biogeochemical processes in intertidal zones of beach aquifers. *Water Resources Research*, 53, 9225–9244. <https://doi.org/10.1002/2017WR021110>
- Heiss, J. W., Puleo, J. A., Ullman, W. J., & Michael, H. A. (2015). Coupled surface-subsurface hydrologic measurements reveal infiltration, recharge, and discharge dynamics across the swash zone of a sandy beach. *Water Resources Research*, 51, 8834–8853. <https://doi.org/10.1002/2015WR017395>
- Heiss, J. W., Ullman, W. J., & Michael, H. A. (2014). Swash zone moisture dynamics and unsaturated infiltration in two sandy beach aquifers. *Estuarine, Coastal and Shelf Science*, 143, 20–31.
- Hirt, C. W., & Nichols, B. D. (1981). Volume of fluid (VOF) method for the dynamics of free boundaries. *Journal of Computational Physics*, 39(1), 201–225.
- Horn, D. P. (2002). Beach groundwater dynamics. *Geomorphology*, 48(1–3), 121–146.
- Horn, D. P. (2006). Measurements and modelling of beach groundwater flow in the swash-zone: A review. *Continental Shelf Research*, 26(5), 622–652.
- Huettel, M., Overholt, W. A., Kostka, J. E., Hagan, C., Kaba, J., Wells, W. B., & Dudley, S. (2018). Degradation of Deepwater Horizon oil buried in a Florida beach influenced by tidal pumping. *Marine Pollution Bulletin*, 126, 488–500. <https://doi.org/10.1016/j.marpolbul.2017.10.061>
- Isern-Fontanet, J., Font, J., García-Ladona, E., Emelianov, M., Millot, C., & Taupier-Letage, I. (2004). Spatial structure of anticyclonic eddies in the Algerian Basin (Mediterranean Sea) analyzed using the Okubo–Weiss parameter. *Deep Sea Research Part II: Topical Studies in Oceanography*, 51(25–26), 3009–3028.

- Jia, J., Bai, J., Gao, H., Wang, W., Yin, S., Wang, D., & Han, L. (2019). Effects of salinity and moisture on sediment net nitrogen mineralization in salt marshes of a Chinese estuary. *Chemosphere*, 228, 174–182. <https://doi.org/10.1016/j.chemosphere.2019.04.006>
- Kim, K. H., Heiss, J. W., Geng, X., & Michael, H. A. (2020). Modeling hydrologic controls on particulate organic carbon contributions to beach aquifer biogeochemical reactivity. *Water Resources Research*, 56, e2020WR027306. <https://doi.org/10.1029/2020WR027306>
- Kim, K. H., Heiss, J. W., Michael, H. A., Cai, W. J., Laattoe, T., Post, V. E., & Ullman, W. J. (2017). Spatial patterns of groundwater biogeochemical reactivity in an intertidal beach aquifer. *Journal of Geophysical Research: Biogeosciences*, 122, 2548–2562. <https://doi.org/10.1002/2017JG003943>
- Kim, K. H., Michael, H. A., Field, E. K., & Ullman, W. J. (2019). Hydrologic shifts create complex transient distributions of particulate organic carbon and biogeochemical responses in beach aquifers. *Journal of Geophysical Research: Biogeosciences*, 124, 3024–3038. <https://doi.org/10.1029/2019JG005114>
- Kitanidis, P. K. (1994). The concept of the dilution index. *Water Resources Research*, 30(7), 2011–2026.
- Kostka, J. E., Prakash, O., Overholt, W. A., Green, S. J., Freyer, G., Canion, A., et al. (2011). Hydrocarbon-degrading bacteria and the bacterial community response in Gulf of Mexico beach sands impacted by the Deepwater Horizon oil spill. *Applied and Environmental Microbiology*, 77(22), 7962–7974. <https://doi.org/10.1128/AEM.05402-11>
- Lässig, C. (2019). Spatial and temporal patterns of NO_3^- in an island beach ecosystem utilizing UV photometry.
- Longuet-Higgins, M., & Smith, N. (1983). Measurement of breaking waves by a surface jump meter. *Journal of Geophysical Research*, 88(C14), 9823–9831.
- Lu, C., Chen, Y., Zhang, C., & Luo, J. (2013). Steady-state freshwater-seawater mixing zone in stratified coastal aquifers. *Journal of Hydrology*, 505, 24–34.
- Malott, S., O'Carroll, D. M., & Robinson, C. E. (2017). Influence of instantaneous and time-averaged groundwater flows induced by waves on the fate of contaminants in a beach aquifer. *Water Resources Research*, 53, 7987–8002. <https://doi.org/10.1002/2017WR020948>
- McArdle, S. B., & McLachlan, A. (1992). Sand beach ecology: Swash features relevant to the macrofauna. *Journal of Coastal Research*, 398–407.
- McLachlan, A. (1983). Sandy beach ecology—A review. In A. McLachlan, & T. Erasmus (Eds.), *Sandy Beaches as Ecosystems* (pp. 321–380). Dordrecht: Springer. https://doi.org/10.1007/978-94-017-2938-3_25
- McLachlan, A., Eliot, I. G., & Clarke, D. J. (1985). Water filtration through reflective microtidal beaches and shallow sublittoral sands and its implications for an inshore ecosystem in Western Australia. *Estuarine, Coastal and Shelf Science*, 21(1), 91–104.
- Meng, H., Salas, J., Green, T., & Ahuja, L. (2006). Scaling analysis of space-time infiltration based on the universal multifractal model. *Journal of Hydrology*, 322(1–4), 220–235.
- Michael, H. A., Scott, K. C., Koneshloo, M., Yu, X., Khan, M. R., & Li, K. (2016). Geologic influence on groundwater salinity drives large seawater circulation through the continental shelf. *Geophysical Research Letters*, 43, 10,782–10,791. <https://doi.org/10.1002/2016GL070863>
- Mohapatra, P., Vijay, R., Pujari, P., Sundaray, S., & Mohanty, B. (2011). Determination of processes affecting groundwater quality in the coastal aquifer beneath Puri City, India: A multivariate statistical approach. *Water Science and Technology*, 64(4), 809–817. <https://doi.org/10.2166/wst.2011.605>
- Molz, F. J., & Boman, G. K. (1993). A fractal-based stochastic interpolation scheme in subsurface hydrology. *Water Resources Research*, 29, 3769–3774.
- Nicholson, R. V., Gillham, R. W., Cherry, J. A., & Reardon, E. J. (1989). Reduction of acid generation in mine tailings through the use of moisture-retaining cover layers as oxygen barriers. *Canadian Geotechnical Journal*, 26(1), 1–8.
- Noëtinger, B. (2000). Computing the effective permeability of log-normal permeability fields using renormalization methods. *Comptes Rendus de l'Académie des Sciences - Series IIa - Earth and Planetary Science*, 331(5), 353–357.
- Okubo, A. (1970). Horizontal dispersion of floatable particles in the vicinity of velocity singularities such as convergences, paper presented at deep sea research and oceanographic abstracts, Elsevier.
- Papoulis, A. (1991). *Probability, random variables, and stochastic processes* (p. 666). New York: McGraw Hill.
- Parisi, G., & Frisch, U. (1985). A multifractal model of intermittency. In M. Ghil, R. Benzi, & G. Parisi (Eds.), *Turbulence and predictability in geophysical fluid dynamics and climate dynamics* (pp. 84–88). New York: North-Holland.
- Pecknold, S., Lovejoy, S., Schertzer, D., Hooge, C., & Malouin, J. (1993). The simulation of universal multifractals, paper presented at Cellular Automata.
- Peitgen, H.-O., & Saupe, D. (1988). *The science of fractal images*. New York, Inc: Springer-Verlag.
- Pool, M., Post, V. E., & Simmons, C. T. (2015). Effects of tidal fluctuations and spatial heterogeneity on mixing and spreading in spatially heterogeneous coastal aquifers. *Water Resources Research*, 51, 1570–1585. <https://doi.org/10.1002/2014WR016068>
- Praveena, S. M., Kwan, O. W., & Aris, A. Z. (2012). Effect of data pre-treatment procedures on principal component analysis: A case study for mangrove surface sediment datasets. *Environmental Monitoring and Assessment*, 184(11), 6855–6868. <https://doi.org/10.1007/s10661-011-2463-2>
- Rakhimbekova, S., O'Carroll, D. M., Andersen, M. S., Wu, M. Z., & Robinson, C. E. (2018). Effect of transient wave forcing on the behavior of arsenic in a nearshore aquifer. *Environmental Science & Technology*, 52(21), 12,338–12,348.
- Robinson, C., Xin, P., Li, L., & Barry, D. A. (2014). Groundwater flow and salt transport in a subterranean estuary driven by intensified wave conditions. *Water Resources Research*, 50, 165–181. <https://doi.org/10.1002/2013WR013813>
- Robinson, C. E., Xin, P., Santos, I. R., Charette, M. A., Li, L., & Barry, D. A. (2018). Groundwater dynamics in subterranean estuaries of coastal unconfined aquifers: Controls on submarine groundwater discharge and chemical inputs to the ocean. *Advances in Water Resources*, 115, 315–331.
- Rooney, D., Brown, K., & Thomas, J. (1998). The effectiveness of capillary barriers to hydraulically isolate salt contaminated soils. *Water, Air, and Soil Pollution*, 104(3–4), 403–411.
- Ross, B. (1990). The diversion capacity of capillary barriers. *Water Resources Research*, 26(10), 2625–2629.
- Santos, I. R., Burnett, W. C., Dittmar, T., Suryaputra, I. G., & Chanton, J. (2009). Tidal pumping drives nutrient and dissolved organic matter dynamics in a Gulf of Mexico subterranean estuary. *Geochimica et Cosmochimica Acta*, 73(5), 1325–1339.
- Santos, I. R., Eyre, B. D., & Huettel, M. (2012). The driving forces of porewater and groundwater flow in permeable coastal sediments: A review. *Estuarine, Coastal and Shelf Science*, 98, 1–15.
- Schertzer, D., & Lovejoy, S. (1987). Physical modeling and analysis of rain and clouds by anisotropic scaling multiplicative processes. *Journal of Geophysical Research*, 92(D8), 9693–9714.
- Schutte, C. A., Joye, S. B., Wilson, A. M., Evans, T., Moore, W. S., & Casciotti, K. (2015). Intense nitrogen cycling in permeable intertidal sediment revealed by a nitrous oxide hot spot. *Global Biogeochemical Cycles*, 29, 1584–1598. <https://doi.org/10.1002/2014GB005052>

- Schutte, C. A., Wilson, A. M., Evans, T., Moore, W. S., & Joye, S. B. (2018). Deep oxygen penetration drives nitrification in intertidal beach sands. *Limnology and Oceanography*, 63(S1), S193–S208.
- Sebben, M. L., Werner, A. D., & Graf, T. (2015). Seawater intrusion in fractured coastal aquifers: A preliminary numerical investigation using a fractured Henry problem. *Advances in Water Resources*, 85, 93–108.
- Shin, B., Bociu, I., Kolton, M., Huettel, M., & Kostka, J. E. (2019). Succession of microbial populations and nitrogen-fixation associated with the biodegradation of sediment-oil-agglomerates buried in a Florida sandy beach. *Scientific Reports*, 9(1), 1–11.
- Siena, M., & Riva, M. (2018). Groundwater withdrawal in randomly heterogeneous coastal aquifers. *Hydrology and Earth System Sciences*, 22(5), 2971–2985.
- Sous, D., Lambert, A., Rey, V., & Michallet, H. (2013). Swash-groundwater dynamics in a sandy beach laboratory experiment. *Coastal Engineering*, 80, 122–136.
- Sous, D., Petitjean, L., Bouchette, F., Rey, V., Meulé, S., Sabatier, F., & Martins, K. (2016). Field evidence of swash groundwater circulation in the microtidal roasty beach, France. *Advances in Water Resources*, 97, 144–155.
- Stormont, J. C., & Anderson, C. E. (1999). Capillary barrier effect from underlying coarser soil layer. *Journal of Geotechnical and Geoenvironmental Engineering*, 125(8), 641–648.
- Tchiguirinskaia, I., Lu, S., Molz, F., Williams, T., & Lavallée, D. (2000). Multifractal versus monofractal analysis of wetland topography. *Stochastic Environmental Research and Risk Assessment*, 14(1), 8–32.
- Tennekoon, L., Boufadel, M. C., Lavallee, D., & Weaver, J. (2003). Multifractal anisotropic scaling of the hydraulic conductivity. *Water Resources Research*, 39(7), 1193. <https://doi.org/10.1029/2002WR001645>
- Tian, Y., Ouyang, H., Gao, Q., Xu, X., Song, M., & Xu, X. (2010). Responses of soil nitrogen mineralization to temperature and moisture in alpine ecosystems on the Tibetan Plateau. *Procedia Environmental Sciences*, 2, 218–224.
- Turner, I. L., Rau, G. C., Austin, M. J., & Andersen, M. S. (2016). Groundwater fluxes and flow paths within coastal barriers: Observations from a large-scale laboratory experiment (BARDEX II). *Coastal Engineering*, 113, 104–116.
- Ullman, W. J., Chang, B., Miller, D. C., & Madsen, J. A. (2003). Groundwater mixing, nutrient diagenesis, and discharges across a sandy beachface, Cape Henlopen, Delaware (USA). *Estuarine, Coastal and Shelf Science*, 57(3), 539–552.
- Van Genuchten, M. T. (1980). A closed-form equation for predicting the hydraulic conductivity of unsaturated soils 1. *Soil Science Society of America Journal*, 44(5), 892–898.
- von Jeetze, P. J., Zarebanadkouki, M., & Carminati, A. (2020). Spatial heterogeneity enables higher root water uptake in dry soil but protracts water stress after transpiration decline: A numerical study. *Water Resources Research*, 56, e2019WR025501. <https://doi.org/10.1029/2019WR025501>
- Waska, H. (2019). Spatial and temporal patterns of pore water chemistry in the inter-tidal zone of a high energy beach. *Frontiers in Marine Science*, 6, 154.
- Weeks, S. W., & Sposito, G. (1998). Mixing and stretching efficiency in steady and unsteady groundwater flows. *Water Resources Research*, 34(12), 3315–3322.
- Weiss, J. (1991). The dynamics of enstrophy transfer in two-dimensional hydrodynamics. *Physica D: Nonlinear Phenomena*, 48(2–3), 273–294.
- Wilcox, D. C. (1993). Turbulence modeling. *DCW Industries*.
- Wilcox, D. C. (1998). *Turbulence Modeling for CFD*. CA: DCW industries La Canada.
- Xin, P., Robinson, C., Li, L., Barry, D. A., & Bakhtyar, R. (2010). Effects of wave forcing on a subterranean estuary. *Water Resources Research*, 46, W12505. <https://doi.org/10.1029/2010WR009632>
- Yadav, B. K., & Hassanzadeh, S. M. (2011). An overview of biodegradation of LNAPLs in coastal (semi)-arid environment. *Water, Air, & Soil Pollution*, 220(1–4), 225–239.
- Yin, S., Bai, J., Wang, W., Zhang, G., Jia, J., Cui, B., & Liu, X. (2019). Effects of soil moisture on carbon mineralization in floodplain wetlands with different flooding frequencies. *Journal of Hydrology*, 574, 1074–1084.